Development of a Hybrid Hydrogel Bio-ink for 3D Printing of Biomimetic Tissue Constructs

By

Andrew Wenger

A thesis

presented to the University of Waterloo

in fulfilment of the

thesis requirement for the degree of

Master of Science

in

Chemistry

Waterloo, Ontario, Canada, 2019

AUTHOR DECLARATION

I hereby declare that I am the sole author of this thesis. This is a true copy of the thesis, including any required final revisions, as accepted by my examiners.

I understand that my thesis may be made electronically available to the public.

Abstract

Colorectal cancer is the 2nd most common form of cancer in Canada. Most colorectal cancer deaths are caused by complications that stem from the metastasis of colorectal cancer to other organs such as the liver. During metastasis, the extravasation step of the metastasis cascade involves the attachment of circulating tumour cells to the endothelial cell layer that coats the inside of human blood vessels and the eventual migration of the cells past this layer. Current tumour extravasation models, used for drug and mechanistic studies, do not accurately reflect the micro-environments found in the human body. Three dimensional bioprinting has become an attractive method to produce extravasation models. This thesis explores the development of a hybrid hydrogel bio-ink consisting of alginate, GelMA and cellulose nanocrystals to create cell scaffolds that can support the growth of a monolayer of endothelial cells. A bio-ink consisting of 2 wt% alginate, 4 wt% GelMA and 6 wt% cellulose nanocrystals was chosen for printability studies and cellular studies for its high shear thinning and low hysteresis in viscosity recovery. Scaffolds designed to mimic a human blood vessel and villi structures in a healthy colon were printed and EA-hy 926 cells were seeded on top. After six days and an additional seeding of cells it was found that the bio-ink could not sustain the growth of a complete mono-layer of EA-hy 926 cells. The high electrostatic repulsion between the negatively charged cell membrane and the negatively charged alginate and cellulose nanocrystals is thought to play a role in the ability of the cells to attach to the scaffold surface. Scaffold treated with poly(L-lysine) were made and EA-hy-926 cells were again seeded on top. This resulted in better cell distribution, but increased instances of cellular elongation suggested a decrease in cellular adhesion. In both poly(L-lysine) treated and un-treated scaffolds the cells were able to attach and proliferate on top of the scaffolds suggesting that with some changes in either the bio-ink's formula, cell seeding densities or post printing

treatments a mono layer of cells could be formed to be used in the production of extravasation models of colorectal cancer.

Acknowledgements

I would like to thank my supervisor Dr. Shirley Tang for all her guidance throughout my research, studies and the writing of this thesis.

To my committee members Dr. Jonathan Blay and Dr. Jean Duhamel thank you for your feedback and guidance throughout my master's studies. Special thanks to Dr. Jonathan Blay, who provided the HCT 116 cells used for my research.

Thank you, Dr. Michael Tam, for providing cellulose nanocrystals and the use of his rheometer along with his grad student Nate Grishkewich for instrument training.

I would like to thank Dr. David Spafford for the use of his confocal microscope and guidance in image acquisition.

I would like to thank Dr. Boxin Zhao for the use of his universal material testing machine and his grad student Penfxiang Si for training me and helping to troubleshoot issues.

Thank you to past and current Tang research group members: Zhi Li, Dr. Yael Zilberman-Simakov, Yuxing Wang, Marko Tanuan, Ciara Azam, Eliana Feygin, Kyle Chu, Hoffman Wang, Joshua Liu, Hossein Golzar, Irfani Ausri and Yun Wu. Special thanks to Yun Wu for her previous research in which this project was based off and all her help with background research and 3D printing. I also want to thank Irfani Ausri for all her help with the editing of this thesis.

Thank you to Ourotech for their financial support in this project and their CEO Duleek Ranatunga for hiring me as a co-op student and getting me interested tissue engineering.

To William Lin, thank you for your helpful instructions in technical writing and the time we worked together at Ourotech.

To my parents Dave and Rose, my siblings Sarah, Tim, my sister in law Steph and my nephew Simon, thank you for always supporting me throughout my time as a grad student. Thank you for understanding when I was too busy to visit and helping me through moments of stress.

Thanks to my significant other Hannah for supporting and encouraging me in the final stages of this thesis and providing music to listen to while working.

My friends and Church community, thank you for helping me to stay grounded and supporting me throughout my research. Especially Trevor Potts, who edited my thesis for spelling and grammar.

And finally, thanks be to God from whom all blessings flow for I wouldn't have been able to do this work without you sustaining me.

Contents

List of Figures:

List of Tables

List of Abbreviations:

3D – Three dimensional
A – Area
A_o – Initial cross-sectional area
APTES – (3-aminopropyl) triethoxysilane
BM – Basement membrane
CAM – Chorioallontoic membrane
CNC – Cellulose nanocrystals
CRC – Colorectal Cancer
dh – Height differential
DMEM – Dulbecco's modified Eagle medium
DOS – degree of substitution
dv – Velocity differential
E – Compression modulus
EA-hy 926 - Hybrid endothelial somatic cell line
ECM – Extracellular matrix
ETHD-1 – ethidium homodimer-1
F – Force
FBS – Fetal bovine serum
G – α-L-guluronic acid (G)
GelMA - Methylacrylated gelatin
HA – Hyaluronan
HCT 116 – Human colorectal tumour cell line
H-NMR – Proton nuclear magnetic resonance
hPS-CMs – Human pluripotent stem cell-derived cardiomyocytes
HSPG – Heparan sulphate proteoglycans
$I_{Gelatin}$ – Integral of HNMR peak for lysine groups in gelatin
I_{GelMA} – Integral of HNMR peak for unreacted lysine groups in GelMa
ISM – Interstitial stroma matrix
K – Flow consistency index
l – Length
LAB – Laser assisted bioprinting
LAP - Lithium phenyl-2,4,6-trimethylbenzoylphosphinate
LMW-HA – Low molecular weight hyaluronan
l_o – Initial length
M – β-D-mannuronic acid
ME – Micro extrusion
MSC – Mesenchymal stem cells
n – Flow behaviour index
PBS – Phosphate buffered saline
PCL – Polycaprolactone
PEG - Polyethylene glycol
PEGDA – Poly-ethylene glycol diacrylate
Q – Volumetric flow rate
R – Radius
RU/SPS - Ruthenium and sodium persulfate photo-initiator system

s - Seconds
STL – stereolithography file
TRY/EDTA - 0.025% trypsin-0.01% ethylenediaminetetraacetic acid solution
TSIM - Tissue structure information modeling software
UMT – Universal material tester
v_p – Printer speed
$\dot{\gamma}$ - Shear rate
$\dot{\gamma}_w$ – Shear rate at the wall of the micro-extrusion nozzle
ε_e – Engineering strain
η – dynamic viscosity
η_{eff} – Effective viscosity
σ_e – Engineering stress
τ – Shear stress

Chapter 1 – Introduction to Colorectal Cancer and 3D Bioprinting

1.1 Colorectal Cancer

The Canadian Cancer society estimated that 206 200 new cases of cancer would be diagnosed in the year 2017. Colorectal cancer (CRC) is the 2nd most common type of cancer in Canada with an expected 26 800 new cases in 2017.[1] There are many factors that contribute to the likelihood that a person will contract CRC. Age is often considered the greatest factor as CRC tends occur in older population with the median age being 70 years old. While not completely understood, heritable factors are suspected to increase the risk of CRC by 35%. The loss of genomic integrity in multiple genetic pathways results in the accumulation of multiple mutations in specific oncogenes and/or tumour suppressor genes.[2] Non-heritable factors such as infectious agents (*e.g. Heliobacter pylori* and *Fusobacterium spp*) have also been associated with an increased risk of CRC.[3] Dietary habits, especially the western diet, are also associated with an increased risk of CRC. Countries who previously had low risk have seen an increase CRC diagnosis due to the increasing shift towards a western diet.[3] The combination of these factors and the increase of senior population in Canada has increased the need for new safe and effective treatments for CRC.[4]

1.1.1 Colorectal Cancer Tumours and Metastases

As seen in Figure 1, a healthy colon/rectum has multiple layers that contain different tissues.[5] The innermost layer is called the mucosa and has a thin layer of epithelial cells called the

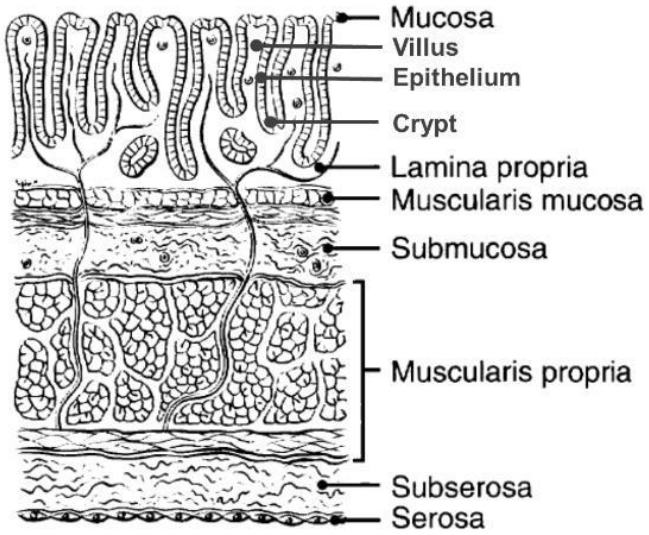

Figure 1: Diagram of normal colorectal tissue. The epithelium is organized along a crypt-villus axis. The bottom of the crypt consists of colon stem and progenitor cells which migrate along eh crypt-villus axis differentiating into different colon epithelial cells.[4]

epithelium. The epithelium is organized along a crypt-villus axis. The bottom of the crypt consists of a pool of colon stem and progenitor cells. As the cells age, they migrate along the crypt-villus axis and differentiate into different colon epithelial lineages. Once these epithelial cells reach the top of the villus they undergo anoikis.[3]

Adenocarcinoma is the most common form of CRC and forms when epithelial cells experience specific genetic and epigenetic mutations. Normal epithelium cells turn into hyperproliferative mucosa which, if untreated, will develop into a benign adenoma. After a long incubation period of approximately 10 years, the benign adenoma can develop into carcinoma and eventually metastasize.[2]

In late stage CRC, the cells can break off the primary tumour and metastasize to other organs in the body, often the liver, and is the most common cause of cancer-related mortality. Approximately 20-25% of CRC patients are diagnosed during the late stages of CRC and about 50% of the patients also suffer from metastasis. Of all the patients whose CRC has metastasized into the liver, only 15-20% are eligible candidates for surgical resection. Hence, the study of the mechanisms involved in CRC metastasis is imperative to improve the survival of patients. [6]

The CRC metastasis process, known as the metastasis cascade, is a complex multi step process where cancerous cells detach from the primary tumour. Once detached, the tumour cells

lose their epithelial polarity and transition into mesenchymal cells. These cells then invade the basement membrane and the extracellular matrix (ECM) to reach the capillaries in a process called intravasation. These tumour cells than travel through blood vessels of the body and go through extravasation in which they enter the tissue surrounding the blood vessel. [6,7]

1.1.2 Tumour and Metastasis Models

Due to CRC's complex nature, *in vitro* models tend to focus on either the primary tumour or specific stages of the metastasis cascade. Cell lines of CRC, both human and murine, have been developed over the years. These cell lines are useful for mechanistic studies that allow for the identification of pathways and targets for cancer therapies. They have well characterized genomes and are relatively inexpensive to culture allowing for rapid experimentation. However, these cell lines are generally cultured in monolayers and are established clonal populations. Thus, they do not accurately reflect the heterogenicity found in CRC tumours and metastasis. Consequently, the cellular pathways associated with the 3D organ structures are not established.[8]

CRC cells can be cultured in organoids to model the 3D environment of colorectal tumours. One possible advantage of CRC organoids is that they can contain the multiple epithelial cells types that are seen in primary tumours.[9] Organoids have also been able to produce functional crypt regions which models the migration of differentiated cells along the crypt-villus axis. It is also possible to produce patient-derived organoids that enables personalized drug testing.[8] On the other hand, a disadvantage with organoids is that they are not able to model tumour vascularization or angiogenesis.[10] By producing vascular tissue, the tumour can readily derive nutrients from the blood stream to promote the growth and proliferation of the tumour cells.[11]

The extravasation of cancer cells from the vasculature structures into the surrounding tissues is considered one of the most important steps within the metastases cascade. Transwell

assay have commonly been used to study extravasation and have determined many molecular mechanisms and components crucial to the extravasation process. This assay involves the seeding of cancer cells into a Transwell filter pore membrane. The cells are then allowed to translocate across the membrane into a well containing chemotaxis factors such as fetal bovine serum (FBS).[12] However, Transwell assays do not accurately reflect the extravasation physiology since the assay utilizes a membrane with 2D circular pores while extravasation occurs along an endothelial junction within the vasculature structures. They are also hemodynamically static and do not have plasma proteins or circulating blood cells that are key to both promoting and counteracting biophysical forces that act on tumour cells within the extravasation process.[12]

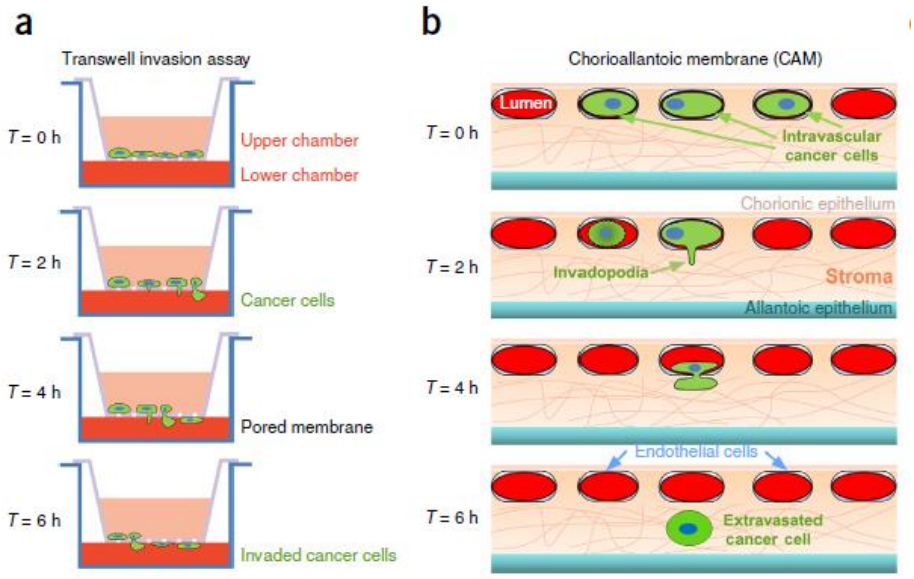

Figure 2: Comparison of Transwell invasion assay and chorioallantoic membrane (CAM). (a) Transwell assay schematic in which cancer cell suspensions are placed into an upper chamber lined with a porous membrane and placed into a lower chamber containing chemotaxis factors. Cells then pass through the porous membrane into the lower chamber allowing for research into molecular mechanisms and components crucial to extravasation process. (b) Schematic of in-vivo extravasation assay using chorioallantoic membranes found in chicken embryos. Cancer cells are injected into the blood vessel of the membrane and allowed to pass through the endothelial cell layer into the surrounding tissue. [12]

Chicken embryos are also used to model the extravasation process. This involves injection of cancer cells into chorioallontoic membrane (CAM) of the chicken embryo. This method has been used to study the efficacy of target genes or drugs that affect cancer cell extravasation. It also allows for the study of metastatic inefficiency because not all the cells will undergo extravasation. The low cost of chicken embryos ($0.50 - $1.00) allows large numbers of CAM assays to be

performed quickly to give more statistical significance when comparing cell types or different drug treatments. A limitation of CAM assays is that the mammalian cells are operating within an avian xenograft microenvironment. Endocrinological factors that are crucial for cancer cell extravasation may not be present and must be considered before using CAM models.[12]

Mice are commonly used as *in vivo* models of the metastasis process of CRC. This usually involves injecting immunocompromised mice with either a CRC cell line or primary patient tumour cells and allowing for the cancer to take a hold. Once a primary tumour is established, cells can detach and metastasize to the liver. However, mice models for metastasis tend to have low predictability and reliability. The mice used are also often immunocompromised, which means that the immune system response is not considered in these models. The time needed for tumours to develop and metastasize can be long resulting in high cost and being labour intensive. Another issue is the difficulty to track tumour growth and the metastasis. Histological evaluation can only be performed post-mortem, so mice models are generally only useful for studying the late stages of metastasis cascade. In order to image metastatic cells, imaging technologies that use genetically-encoded Aequorea victoria green fluorescent proteins in the tumour cells have allowed for the tracking of individual metastasis cells giving more insight into the early stages of liver metastasis.[6]

1.1.3 Extracellular Matrix Components

The ECM is a highly organized three-dimensional structure that plays a critical role in maintaining tissue integrity, regulating cell migration, cellular differentiation, and proliferation.[13] It also acts as a reservoir for cytokines and growth factors needed by the cells.[14] The ECM is divided into the basement membrane (BM) and the interstitial stroma matrix (ISM). The BM consists of thin sheets that surround the epithelial or endothelial cells, nerves and muscle cells.[13]

This thin layer is used to separate the cells from the ISM, which is the material that fills the interstitial space between cells.[14]

The CRC ECM is composed of five predominant classes of macromolecules: collagen, laminin, fibronectin, proteoglycan, and hyaluronan. Collagen type I is the most prominent protein in the human body and is found in the BM and ISM to provide structural support for most soft tissues.[13] In tumours, type I collagen inhibits differentiation and increases clonogenicity since it promotes the expression of stem cell markers.[15]

1.1.3.1 Laminins

Laminins are three-chain proteins that play an important role in the BM. They are involved in the differentiation, migration, and adhesion of CRC cells.[13] Laminin-1 has been shown to stabilize motility structures which promotes tumour cell migration.[16] Laminin-332 is usually not found in carcinomas but is expressed in premalignant tumours. Smad4 is a tumour suppressor gene which also encodes the positive transcription regulator for the genes that encode laminin-332. In late stages of the premalignant tumours Smad4 loses its functionality, resulting in a loss of laminin-332.[17]

1.1.3.2 Fibronectins

Fibronectins are high-molecular weight glycoproteins. They can be found in the ECM in insoluble form as well as bodily fluids in soluble form. Fibronectins can bind to other ECM components such as collagens, and glycosaminoglycan as well as cell surface receptors called integrins.[13] Ding J *et al*. demonstrated that increasing the concentration of fibronectin in Colo320 cells promoted cell invasion by facilitating the expression of focal adhesion kinase.[18]

1.1.3.3 Proteoglycans

Proteoglycans are glycosylated proteins with anionic glycosaminoglycans covalently bonded. The physiochemical characteristic of the glycosaminoglycan components helps to keep

the tissue hydrated and increase swelling pressure to allow the tissue to withstand compressional forces.[19] Syndecan-1 is a proteoglycan that is associated with cell-cell and cell-ECM adhesion and also functions as a growth factor coreceptor. In CRC, Syndecan-1 is down-regulated and is correlated with metastasis to local lymph nodes.[20]

1.1.3.4 Hyaluronan

Hyaluronan (HA), synonymous with hyaluronic acid and hyaluronate, is an anionic polysaccharide that plays a structural role in many connective tissues.[13] HA has been shown to enhance colorectal tumour cell proliferation and motility in *in vitro* and *in vivo* studies.[21,22] There is some evidence that high molecular weight HA can confer drug resistant properties to cells in culture.[23]

1.2 3D Bioprinting

Three dimensional (3D) bioprinting is an attractive method for producing CRC and metastasis models. Based on additive manufacturing techniques used with plastics and ceramics, 3D bioprinting applies these to biological systems to create 3D structures that mimic tissues such as bone, skin, cardiovascular system, and cartilage. These systems use materials that mimic the ECM of the tissue mixed with cell media and growth factors to allow cells to thrive in the artificial tissue.

1.2.1 Deposition Methods

The three major deposition methods for 3D bioprinting are inkjet, laser-assisted, and extrusion-based. Inkjet bioprinting prints by depositing controlled volumes of bio-ink at specified locations. These droplets are then solidified either through chemical or photo crosslinking methods. The droplet volume is controlled either through thermal or acoustic methods. In thermal inkjet printers, a droplet is expelled from the printer head by air pressure produced by the vaporization of water when the bio-ink is heated up at the printer nozzle. The localized heater causes the droplets' temperature to increase slightly but has been shown to have little to no effect on the viability of mammalian cells. Acoustic inkjet printers use either a piezoelectric actuator or an ultrasonic wave to produce the droplets. This prevents the cells from being subjected to the increased temperatures and pressures associated with heated inkjets. However, acoustic damage to the cell membrane can occur if the frequencies are not properly chosen.[24]

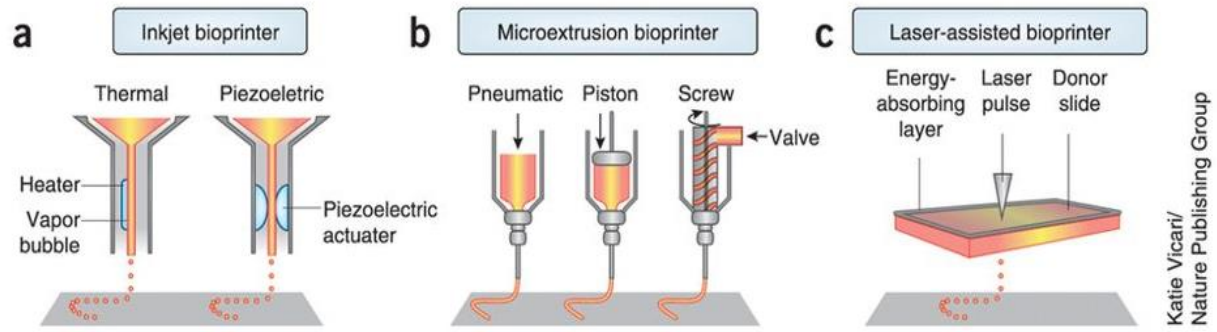

Figure 3: Schematics of bioprinting deposition methods. (a) Formation of droplets through thermal heater and piezoelectric actuator. (b) Formation of filaments through pneumatic, piston or screw extrusion methods. (c) Formation of fine droplets using laser absorbing layer.[24]

Laser-assisted bioprinting (LAB) works by using focused laser pulses directed at a laser energy-absorbing layer, such as gold or titanium, on a glass surface (ribbon) with another layer of biological materials such as cells and hydrogels. The laser energy-absorbing layer transfers the energy from the laser to the biological material to create a high-pressure bubble that propels the biological material onto a collector substrate. The use of the laser allows for high patterning

resolution with materials in a wide range of viscosities. LAB also uses a nozzle-less system that avoids the issue of nozzles clogging that is associated with the other systems. One issue with LAB is that each cell type or material must have its own ribbon which must be interchanged throughout the printing process that slows down the overall output.[24]

Micro-extrusion (ME) is a robot-controlled system that extrudes material onto a substrate through a ME nozzle to form continuous filaments. ME printers consist of a dispensing head and a stage which can be moved in three dimensions. The ME printer can also contain systems for temperature control, humidity, and light sources for photo-crosslinking. The extrusion of biological material is usually controlled through a pneumatic or mechanical system. Pneumatic systems generally have a simpler drive-mechanism but can have delays due to the compression of the gas in the system. Mechanical systems such as pistons or screws have more direct control over the extrusion of the material but have smaller and more complex components which are prone to breaking under high stresses. [24]

Each deposition method has its advantages and disadvantages. Inkjet bioprinters tend to be relatively inexpensive as they can be made with commercially available 2D ink-based printers by adding an electrically controlled elevator stage. Despite their low costs, inkjet bioprinters are more prone to exposing cells to mechanical and thermal stress, low droplet directionality, non-uniform droplet size, frequent clogging, and unreliable cell encapsulation. LAB's high resolution makes it ideal for printing complex patterns, but they are prone to slow flow rates and metallic residues from the laser-energy absorbing layer. LAB's are also associated with high costs making them undesirable for basic tissue engineering research. The ME bioprinter's ability to deposit high cell densities allow it to produce tissue constructs with physiological cell densities. Cell viability is the

major issue with ME bioprinters as the extrusion of the material out of the nozzle can cause high shear stress that damages cell membranes. [24]

ME was chosen as the preferred printing process to develop a CRC extravasation models. The ability to print high cell density tissue constructs means that the time needed for model to reach physiological cell densities may be decreased allowing for faster drug testing throughput and mechanistic studies.

1.3 Cell Scaffold and Bio-ink Compositions

For a material to be used as a bio-ink it must have the proper rheological properties and gelation methods to be printable. The materials must also be biocompatible and encourage cell proliferation. The rate of degradation of the scaffold materials must be similar to the cellular ECM production in order to maintain the shape of the scaffold. The by-products that are produced from the degradation of the scaffolds must not be cytotoxic and not affect the cells' ability to function. Since cells also respond to the biophysical properties of the scaffolds that they are grown in, the materials used must therefore have similar structural and mechanical properties to the desired tissue.[25]

1.3.1 Synthetic

Synthetic polymers, such as polycaprolactone (PCL) and polyethylene glycol (PEG) have been used to create cellular scaffolds. Synthetic polymers are attractive cellular scaffolds materials because the molecular weight, functional groups, monomer hydrophobicity/hydrophilicity and crosslinking density can be controlled. This allows for precise control over their chemical and physical properties. However, they do not have any natural cell attachment sites, which must be artificially added to synthetic polymers to facilitate cell adherence.[26]

PCL is a melt-cure polymer that can be melted and extruded at 60°C resulting in a rigid cell scaffold. The increased temperature of PCL printing means that cells cannot be embedded into the polymer during printing. As previously stated, PCL does not contain any natural attachment sites for cells and is generally printed in conjunction with natural hydrogels to create a strong bioactive scaffold. Since mammalian cells do not produce enzymes to degrade PCL, the degradation of PCL is facilitated through hydrolytic cleavage, making it ideal for long-term implantable devices.[26] Using PCL and poly(lactide-co-caprolactone) as support structure and fibrin hydrogel for cell delivery, Zhang *et al.* 3D printed cell scaffolds that mimic the urethra of rabbits and they were able to maintain 80% cell viability of both urothelial cells and smooth muscle cells for over seven days.[27]

On the other hand, the use of PEG for cell scaffolds requires it to be modified. PEG is commonly modified with acrylate groups to create a photopolymerizable poly(ethylene glycol) diacrylate (PEGDA). By controlling the amount of acrylate addition along with the irradiation time, the physical properties of the hydrogel can be fine-tuned to match the physical properties of the desired tissue. Since PEGDA can be polymerized at physiological temperatures, cells can be added to PEGDA solution before bioprinting to allow cell encapsulation.[26,28]As seen with PCL, PEGDA does not contain cell adhesion sites, which must be added into the hydrogels either through chemical addition or creating hybrid hydrogels that incorporate natural polymers such as collagen or gelatin.[26]

Koffler *et al.* developed cells scaffolds containing PEGDA and methylacrylated gelatin (GelMA) to produce scaffolds that mimics the spinal chord architecture of rodents. After loading the scaffolds with neural progenitor cells and implanting the scaffold into rodents with complete spinal cord injury, they observed that the implanted neural progenitor cells extended axons out of

the scaffold and into the spinal chord of the rodent to restore some synaptic transmission and improving functionality.[29]

1.3.2 Natural Polymers

While synthetic polymers have the advantage of possessing controllable properties, natural polymers tend to be more bioactive. Thus, cells interact with these polymers in ways observed in the natural tissues. Many natural polymers, such as collagen and hyaluronic acid, used for cell scaffolds are degraded with enzymes produced by the cells and can be used by the cells to function and build their own ECM. [24]

1.3.2.1 Collagen

Collagen is a key structural protein found in the ECM of most tissues in the human body. Collagen molecules are made up of three polypeptide α-chains. Each chain creates a left-handed polyproline II-type helix. These three helices form a righ-thanded triple helix that is held together through hydrogen, intramolecular van de Waals, and some covalent bonds. This triple helix structure then forms microfibrils and fibrils which further assemble into collagen fibres. [30] Collagen contains arginine-glycine-aspartic acid amino acid sequences that allow cells to bind to the collagen and proliferate throughout the hydrogel. Collagen also contains high numbers of hydrophobic peptide motifs that can cause water exclusion and contraction, resulting in a decrease in nutrient and gas diffusion. [26] For instance, Wang *et al*. used collagen hydrogels that were micropatterned with crypt and villi structures to generate an *in vivo* self regenerating human small intestine epithelium cell layer. This cell layer exhibited similar characteristic to what is seen in the small intestine such as the migration of differentiated cells from the crypt to the villi.[31]

1.3.2.2 Gelatin

There are two types of gelatin that are formed through the hydrolytic degradation of collagen. Type A gelatin comes from collagen found in pig skin and is hydrolyzed through an acidic process. Type B gelatin is made from collagen found in bovine skin which goes through a basic hydrolysis process called liming. The only major difference between type A and type B gelatin is that type A gelatin has a nitrogen content of 18.5% while type B has only 18.0% due to the loss of amide groups. [32] Gelatin can form hydrogels at physiological pH by heating it to above 40°C and allowing it to cool. This causes a thermal rearrangement of the gelatin molecules allowing some to form triple helices like those found in collagen. The main disadvantage is that these hydrogels have relatively low melting points, between 30 and 35°C, making them unusable for cell culture where the temperature needs to be maintained around 37°C. To overcome the low melting points of gelatin, crosslinkers are used to covalently bond the gelatin chains to increase the strength of the hydrogels at higher temperatures. [26]

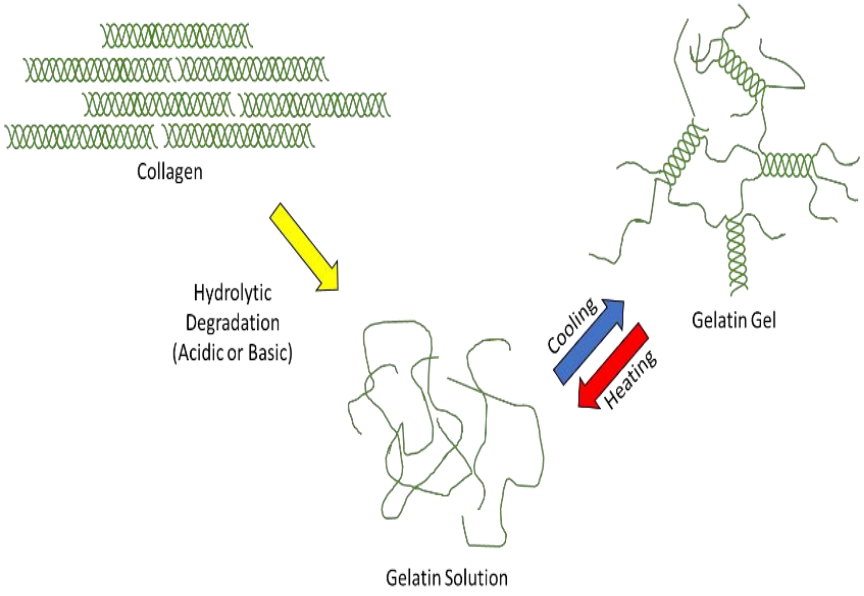

Figure 4: Schematic of gelatin formation from collagen through acid or basic hydrolysis. Gelation of gelatin occurs through the formation of triple helices like those found in collagen. These triple helices are thermal sensitive resulting in gelatins low melting point ranging from 30 to 35°C

By combining regular gelatin with GelMA, Yin *et al.* were able to create a printable hydrogel by printing at low temperature on a cooling printer bed to take advantage of gelatins

thermal crosslinking mechanisms. Printed layers were permanently crosslinked using a lithium phenyl-2,4,6-trimethylbenzoylphosphinate (LAP) as a photo-initiator and constant irradiation with a UV light source throughout the printing process. This method allowed them to use low concentrations of Gelatin/GelMA, which has been shown to help improve cell proliferation and functionality.[33]

1.3.2.3 Hyaluronic Acid

HA is the simplest glycosaminoglycan, consisting of repeating disaccharide units of β-1,4 linked D-glucuronic acid and N-acetyl-D-glucosamine connected through β-1,3 glycosidic bonds. The molecular weight of HA can range from just a few disaccharides to greater than 106 Da. HA was originally thought to be an inert structural polymer but has been shown to play an important role in cell-cell communication. When ECM homeostasis is disrupted, high molecular weight HA is degraded by hyaluronidases and reactive oxygen species into low molecular weight HA (LMW-HA). LMW-HA can then be further degraded into oligosaccharide. Consequently, downstream cellular signalling is affected by the size of hyaluronic acid fragments that attach to cell receptors.[34]

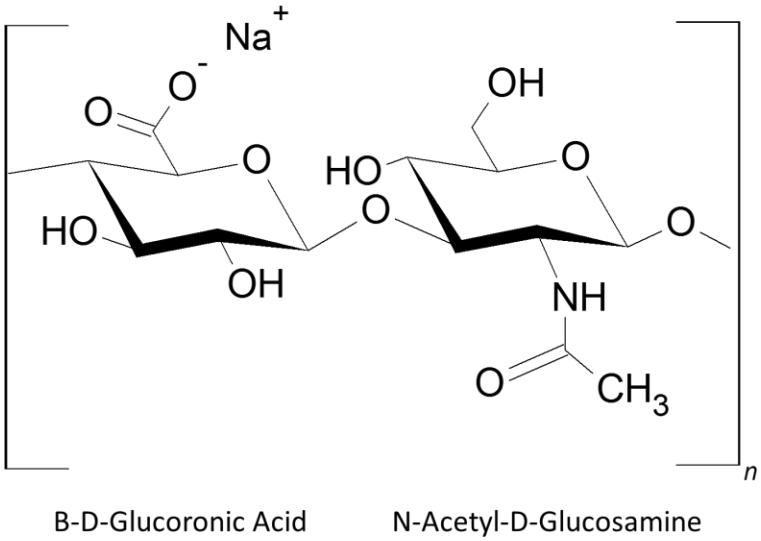

Figure 5: Repeating disaccharide unit of hyaluronic acid.

HA is a linear polymer and is naturally shear-thinning.[35] Even at high concentrations, HA does not form a hydrogel but rather forms a highly viscous fluid.[36] Crosslinking mechanisms are used with HA to produce hydrogels. Highley *et al.* modified two batches of HA with either β-cyclodextrin or adamantane. When these two modified HAs are mixed, at molar equivalents of β-cyclodextrin and adamantane,

they form physical crosslinks through hydrophobic interactions that form between the hydrophobic interior of the β-cyclodextrin and the hydrophobic adamantane.[37]

1.3.2.4 Alginate

Alginate is an anionic polysaccharide, derived from brown seaweed or brown algae. Alginate is a copolymer of (1-4) β-D-mannuronic acid (M) and (1-4) α-L-guluronic acid (G) in their pyranosic conformation. There are three polymer block types that occur in alginate. The first block is alternating MG blocks which is associated with the most flexible parts of the chains. GG blocks are associated with the formation of complexes with divalent counterions such as Ca^{2+}, Ba^{2+} and Sr^{2+}. Lastly, MM groups forms the stiffer sections of the polymer.[38] Mammalian cells do not produce enzymes that catalyze β(1-4)-glycosidic bonds, which increases the residence time of the hydrogels *in vitro* and *in vivo*. [39] While alginate can crosslink through the formation of complexes with divalent counterions, these hydrogels generally have low mechanical strength and thus additional modifications need to be made to create scaffolds with the proper mechanical properties. [39] In 2015 Tabriz *et al.* demonstrated a micro-extrusion technique that allows for the printing of cell-laden

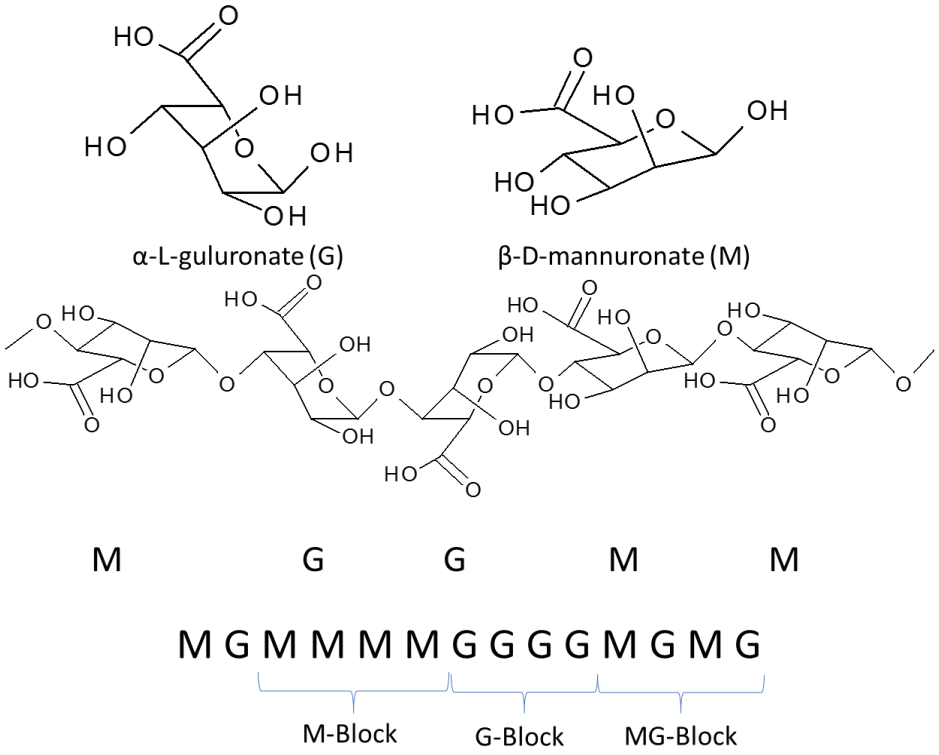

Figure 6: Alginate monomers and polymer structures. MG blocks are associated with flexible sections of the alginate polymer while MM blocks are associated with stiffer sections of the polymer. The ability of alginate to crosslinking with divalent cations such as Ca^{2+} is caused by the interactions with carboxylate groups found in the GG sections.

alginate hydrogels. After each layer of the scaffold was printed the printing plate would submerge the previous layer in cell media containing calcium chloride. Using this technique, they were able to print branching vasculature structures seeded with U87- MG cells and maintain viability over 88% over a period of 11 days.[40]

1.3.2.5 Chitosan

Chitosan is a linear amino-polysaccharide that contains glucosamine and N-acetyl-glucosamine. Chitin is the precursor of chitosan and is the second most prevalent form of polymerized carbon in nature. Chitosan is produced through the deacetylation of chitin through alkali treatments in aqueous solutions. While chitin is insoluble, chitosan is soluble in dilute acidic aqueous solutions. Pure chitosan is not very useful for cell scaffolds as it does not contain cell attachment sites. However, hybrid gels with chitosan and other biopolymers, such as gelatin and hyaluronic acid, have been used to create promising cell scaffolds for tissue engineering.[41] For instance, Demitras *et al.* printed MC3T3-E1 pre-osteoblast cells on chitosan with hydroxyapatite and found that after 21 days of culture that the cells had mineralized and differentiated osteogenically.[42]

1.3.2.6 Cellulose

Cellulose is the most prevalent form of polymerized carbon in the world and is found in the cell walls of plants. The basic structure of cellulose is a linear polymer of β(1-4)-D-glucose.[28] Unmodified cellulose has a very low solubility due to its ability to form crystalline micro-fibrils which are stabilized by hydrogen bonds. [39] Through the addition of methyl groups and other

reactant groups, the solubility of cellulose increases and can be used to produce modified cellulose hydrogels.[43]

As previously stated, mammalian cells do not produce the enzymes needed to break down the β(1-4)-glycosidic bonds. Consequently, the degradation of cellulose is facilitated through hydrolysis which is slow at physiological condition. This increases the residence time of cellulose hydrogels for *in vivo* and *in vitro* experiments.[44]

Often cellulose scaffolds are created through the decellularization of plant-based materials. Using spinach leaves as their starting point Gershlak *et al.* developed a scaffold in which nutrient can be perfused using the spinach's natural vasculature structures. They consequently were then able to recellularize the scaffold with human umbilical vein endothelial cells, human mesenchymal stem cells and human pluripotent stem cell-derived cardiomyocytes (hPS-CMs). In their experiments with hPS-CMs they observed spontaneous contraction after five days of culturing them in the spinach scaffold. [45]

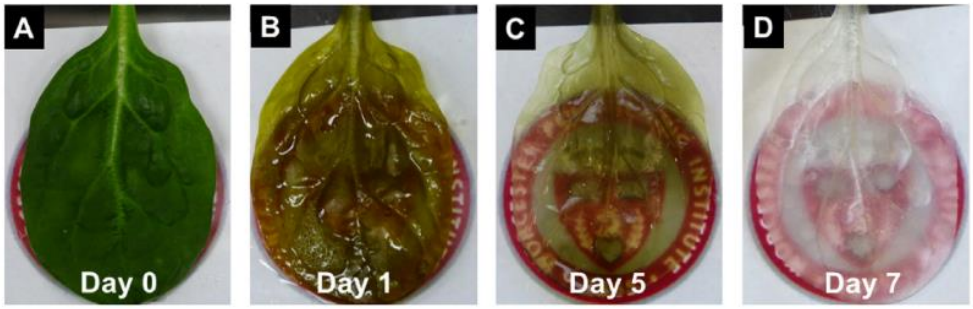

Figure 7: Time lapse of the decellurization of a spinach leaf to produce cellulose scaffolds with naturally formed vasculature structure allowing for the perfusion of nutrients.[41]

1.3.3 Composite Bio-inks

As can be seen with the previous examples of hydrogels, most polymers in their pure form do not possess all the mechanical, rheological, and biological characteristics that are needed for 3D bioprinting. Either modifications must be made to the polymers to give them the desired characteristics or the polymers must be combined into composite bio-inks that use the characteristics of the individual polymers to enhance the overall bio-inks capabilities.

1.3.3.1 Cellulose Nanocrystals

The introduction of nano-filler materials is often used to improve the mechanical and rheological properties in composite materials. Cellulose nanocrystals (CNCs) are made through the removal of cellulose amorphous regions from the crystalline domains through strong acid hydrolysis. The remaining crystallin domains form a nano-material with a high aspect ratio which is added to polymers to change their mechanical strength and rheological properties.[46]

The highly crystalline CNCs act as rigid rods that interact with non-rigid polymer chains creating a chain-crystal-chain network that can transfer energy from one crystal to another. This results in mechanical forces being homogeneously distributed throughout the hydrogel increasing its overall strength.[47]

CNCs induce shear thinning in polymer solutions. When a shear stress is applied to a polymer solution that contains CNC, the CNCs at the shear surface align themselves longitudinally in the direction of the shear stress. This causes the CNCs to slip against each other resulting in an apparent decrease in viscosity. Once the shear stress is removed, the CNCs returns to random orientations and the polymer solutions begins to solidify.[48]

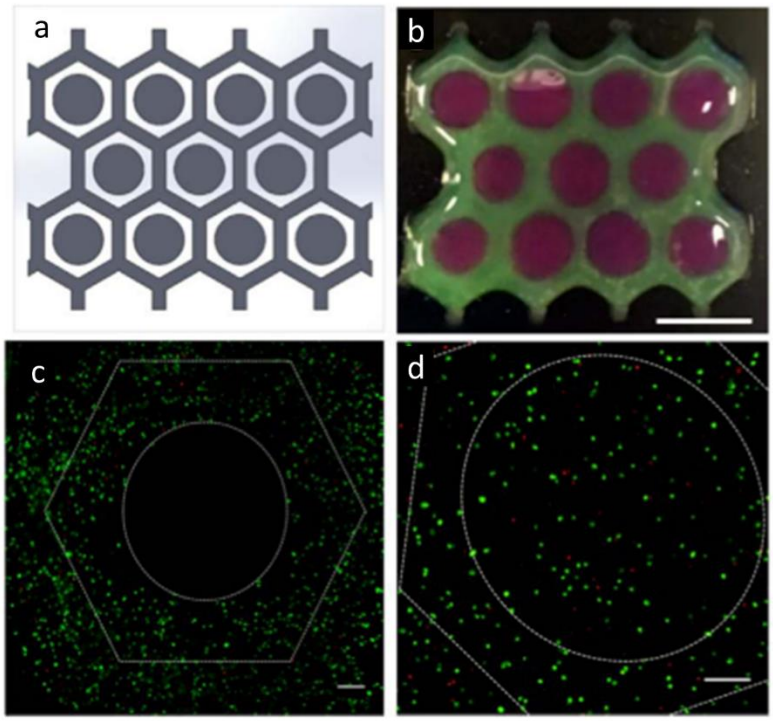

Figure 8: Liver mimetic tissue constructs with fibroblast and heptomic cells. (a) Top down schematic of liver-mimetic constructs. (b) 2% Alginate 4% CNC printed constructs with food dye to distinguish fibroblast cell laden bio-ink (green) and hepatoma cell laden bio-ink (pink). (c&d) Live/dead fluorescent images of bio-printed constructs. (c) Fibroblast only. (d) Fibroblast and hepatoma cells.[42]

The ability of CNCs to produce shear-thinning in polymer solutions is very useful for 3D-bioprinting. The ability to recover from shear-thinning means that bio-inks can maintain their shape long enough for the crosslinking methods to be employed. Furthermore, the increased slippage at the wall can cause plug flow to occur during the deposition process. During plug flow, the shear stress only occurs at the wall surface and little to no shear occurs throughout the rest of the hydrogel. This is ideal for cell encapsulations as only the cells that are near the walls of the nozzle and syringe will be affected by the shear stress during the printing process.[49]

Previous research done in the Tang lab by Wu *et al.* combined cellulose nanocrystals with alginate to produce bio-inks in which fibroblasts and hepatoma cells were printed together in a liver-mimetic honey comb structure. This alginate-CNC bio-ink was able to extrude through a 100 μm diameter extrusion nozzle with minimal cell damage and without clogging allowing for prints with high fidelity. It is speculated that because both alginate and cellulose do not contain cell attachment sites there was a decrease of cell viability to 59% for fibroblast and 50% for hepatoma cells after 3 days.[50]

1.4 Bio-ink Characteristics

1.4.1 Rheology

Rheology is the measurement of the deformation of a material caused by force acting on it. Rheological methods are used in bioprinting in order to predict the behaviour of a bio-ink during the extrusion process. There are different rheometer geometries used for rheological testing, but they all work on similar principles as those used in parallel plate rheometers. Parallel plate rheometers use two plates separated at by a known height, in which the bottom one is fixed and the top plate, with a known area, is moved by a force at a measurable velocity. The shear stress (τ) is then defined as the force (F) acting on an area (A) to effect movement within a liquid. [51]

$$\tau = \frac{F}{A} = \left[\frac{N}{m^2}\right] = [Pa] \tag{1.1}$$

Applying shear stress causes laminar shear flow to be generated between the two plates. This results in a velocity gradient between the two plates with a maximum velocity at the moving top plate and a stationary layer at the bottom plate. The shear rate ($\dot{\gamma}$) is defined as the velocity differential (*dv*) over the height differential (*dh*). [51]

$$\dot{\gamma} = \frac{dv}{dh} = \left[\frac{\frac{m}{s}}{m}\right] = [s^{-1}] \tag{1.2}$$

The viscosity of a fluid describes its resistance to flow. The higher the viscosity the more force is needed for the fluid to flow. For laminar flow the dynamic viscosity (η) of a fluid is equal to the ratio of the shear stress over the shear rate. [51]

$$\eta = \frac{\tau}{\dot{\gamma}} = \left[\frac{Pa}{s^{-1}}\right] = [Pa \cdot s] \tag{1.3}$$

In Newtonian fluids the viscosity is independent of the shear rate.[51]

$$\eta = \frac{\tau}{\dot{\gamma}} = const \tag{1.4}$$

In many materials there is often a large decrease in viscosity as the shear rate increases, known as shear thinning. These materials are known as pseudoplastics and their viscosity is modeled using the OstWal De Wael expression, where K is the flow consistency index [Pa·s^n]and n is the flow behaviour index [dimensionless]. [51]

$$\tau = K \times \dot{\gamma}^n \tag{1.5}$$

Substituting Equation 1.5 into Equation 1.4, the power law model for the effective viscosity (η_{eff}) is acquired as: [51]

$$\eta_{eff} = K \times \dot{\gamma}^{n-1} \tag{1.6}$$

In bioprinting, a high shear stress can cause damage to the cell membranes. The shear thinning ability of the bio-ink is important as it reduces the amount of shear stress imparted on the cells during the extrusion process. If laminar flow occurs during extrusion, we can expect the highest amount of shear stress at the wall of the micro-nozzle. Drawing from equations developed for capillary rheometry, *Bruneaux et al.* developed an equation for the shear rate at the wall of a micro nozzle,[52]

$$\dot{\gamma}_w = \frac{4Q}{\pi R^3}\left(\frac{3+b}{4}\right) \tag{1.7}$$

where Q is the volumetric flow rate which can be determined using the printing speed (v_p) and the micro nozzle radius (R). The parameter b is the inverse of the flow behaviour index.[52]

$$Q = \pi R^2 v_p \tag{1.8}$$

$$b = \frac{1}{n} \tag{1.9}$$

Substituting Equations 1.8 and 1.9 into 1.7 yields the relationship between the shear rate at the wall and the printing speed is shown in Equation 1.10.

$$\dot{\gamma}_w = \frac{v_p}{R}\left(\frac{3+b}{4}\right) \tag{1.10}$$

By performing a constant shear-rate experiment, the flow behaviour index can be acquired from the viscosity curves. Afterwards, the shear stress that cells experience at the wall of the micro-nozzle can be determined.[52]

1.4.2 Crosslinking

For a bio-ink to produce a solid hydrogel, it must form crosslinks between the different polymer chains. Many polymers form weak hydrogels through spontaneous entanglement of the polymer chains. Some polymers, such as gelatin and collagen, can further entangle through the formation of helices to produce a physically crosslinked polymer network. These helices are often temperature sensitive, which makes them not ideal for bio-inks. Some polymers, such as alginate, can form physical complexes with certain ions to bridge the polymer chains and form a polymer network. These physical crosslinks are often sensitive to the surrounding environment and are easily broken. Therefore, to produce permanent hydrogels that can resist changes to the environment, covalent bonds need to be formed between the polymer chains.[53] Chemical crosslinking methods such as with glutaraldehyde have been extensively used to form polymer networks. The disadvantage with these methods is that the chemicals are often cytotoxic to cells and thus the excess must be removed before cells are introduced to the system.[54]

Photopolymerization is often used to crosslink bio-inks. This involves the addition of photo-crosslinkable functional groups to polymer chains. These functional materials are activated using photo-initiators to produce free radicals that interact with functional groups to form covalent bonds between the polymer chains. A common approach used for hydrogels is the addition of vinyl groups to polymer chains often in the form of methacrylate along with either Irgacure 2959 (Irg) or Lithium phenyl-2,4,6-trimethylbenzoylphosphinate (LAP) photoinitiators.

1.4.2 Mechanical Strength

There are many methods used to test the mechanical strength of a hydrogel including tension, compression, shear rheometry and dynamic mechanical analysis. The most commonly reported methods used in hydrogel research are usually tension or compression testing. In tension tests, the samples are held at both ends while they are being pulled apart and the force is measured. When the hydrogel is hydrated, the sample often cannot be gripped properly throughout the test leading to false measurements. Unconfined compression tests are done between two solid plates that measure the force imparted by the sample as the plates compress the sample. In both cases load-displacement data is produced which is then converted to stress-strain data.

Stress (σ) is defined as the force (F) applied over an area (A).[55]

$$\sigma = \frac{F}{A} \tag{1.15}$$

The area in which the force is applied to throughout the test changes due to the stretching or compression of the sample. Since these changes can be hard to measure, the engineering stress (σ_e) utilizes the initial cross-section (A_o) area rather than the true cross-sectional area.[55]

$$\sigma_e = \frac{F}{A_o} \tag{1.16}$$

Strain is the measurement of deformation of a material as a force is applied. These deformations occur in a 3D space and can be difficult to measure. In order to simplify the measurements, we can use engineering strain (ε_e) which compares the length of the material (l) to the initial material length (l_o) in the axis of compression or tension.[55]

$$\varepsilon_e = \frac{l - l_o}{l_o} \tag{1.17}$$

While the engineering stress and strain do not accurately reflect the true stress and strain throughout the measurements, they are considered accurate for the initial strain sections. Since this section is linear, the compression modulus (E) can be determined using Hooke's law.[55]

$$\sigma_e = E\varepsilon_e \tag{1.18}$$

Chapter 2 – Bio-ink Composition and Characterization

2.1 Introduction – The Need for Gelatin

It has been shown that the introduction of CNCs to alginate helps to improve the mechanical and rheological properties and is able to be used as a bio-ink to print fibroblast cells. The issue with this system is that alginate and CNCs both lack cell adhesion sites. This results in cell not proliferating throughout the hydrogel.[50] As mentioned in section 1.3.2.2, gelatin is the product of the hydrolysis of collagen and contains arginine-glycine-aspartic acid amino acid sequences that are a common cell binding site. Simply adding gelatin to the bio-inks may not be useful as gelatin is a thermal responsive polymer that crosslinks with itself at temperatures below 35°C and therefore would quickly leach out of the scaffolds when exposed to the 37°C and 5% CO_2 incubation conditions normally associated with mammalian cell cultures. By converting the gelatin to GelMA, a gelatin network that is covalently crosslinked would be formed and the gelatin will not simply leach out of the scaffolds when incubated.

This chapter explores the rheological, mechanical and printability of bio-inks that are based on the research previously conducted in the Tang lab with the addition of GelMA. GelMA is first produced and the degree of substitution (DOS) of the methacrylate anhydride to the lysine groups is discussed. Bio-inks containing alginate, GelMA and CNCs are produced and the rheological properties and mechanical strengths are measured followed by a discussion on how these measurements may affect bioprinting. Bio-ink printability is compared with a polymer concentration equivalent alginate and GelMA bio-ink along with a discussion on different methods to improve bio-ink fidelity.

2.2 Materials and Methods

2.2.1 Materials

Gelatin type A 300 bloom from porcine skin, methacrylic anhydride, Calcium Chloride ($CaCl_2$), 30 wt% hydrogen peroxide, (3-aminopropyl) triethoxysilane (APTES), lithium phenyl-2,4,6-trimethylbenzoylphosphinate (LAP) and deuterium oxide were purchased from Sigma Aldrich. Sulphuric Acid (A300-212) was purchased from Fisher Scientific. FMC corporation provided a product sample of their pharmaceutical grade sodium alginate (PROTANAL LF 10/60FT) with 60-70% G residues. A sample of cellulose nanocrystals hydrolyzed from wood was donated by Professor Michael Tam from the Department of Chemical Engineering at the University of Waterloo.

2.2.2 – Synthesis of GelMA

GelMA was synthesised using the protocol developed by Shirahama *et al.* Briefly, 10 g of gelatin was soaked in 100 mL of 0.25 M CB buffer at a pH of 9 in a round bottom flask. While stirring the soaked gelatin was then placed in a water bath and the temperature of the gelatin was raised to 50 °C. Methacrylic anhydride (1 mL) was added dropwise and the speed of the stirring was adjusted to prevent the phase separation of methacrylic anhydride while minimizing the amount of air bubbles being added to the solution. The reaction between the gelatin and methacrylic anhydride was carried out for three hours. The reaction was stopped through the addition of hydrochloric acid to reach a pH of 7.4.[56] The resulting solution was then centrifuged in 50 mL falcon tubes for 10 minutes at 3250 xg to remove excess methacrylic anhydride. The supernatant was then decanted into a beaker and 200 mL of 50°C ultrapure water was mixed in. The GelMA solution was placed into cellulose dialysis tubing with a molecular cut-off of 14 000 Da (Sigma Aldrich D9402) and dialyzed against deionized (DI) water for 7 days with water

changes occurring 2-3 times per day. The GelMA solution was then placed in 50 mL falcon tubes, flash frozen in liquid N_2 and lyophilized for three days. Lyophilized GelMA foam was then dissolved in deuterium oxide at 50 mg/mL and analyzed using proton nuclear magnetic resonance (H-NMR).

2.2.3 – Bio-ink Mixing and Characterization

2.2.3.1 – Bio-ink Mixing

Alginate and GelMA were mixed together in ultrapure water at 2 wt% and 4 wt%, respectfully, along with either 6, 5 and 4 wt% of cellulose nanocrystals to form bio-inks. Bio-inks were labelled based on their content (wt% Alg: wt% GelMA: wt% CNC).The order in which the three polymers were mixed changes the rheological properties of the bio-ink. The following mixing procedure was developed to form a bio-ink that was most likely to maintain its shape after printing but could sheer thin to prevent cell damage. A detailed discussion on the polymer mixing order can be found in appendix A.

Depending on the formula of the bio-ink, either 200.0 ± 0.1 mg, 250.0 ± 0.1 mg or 300.0 ± 0.1 mg of cellulose nanocrystals were weighed and added to 4 mL of ultrapure water. The CNCs and water were then vortexed for five minutes and the mixture was sonicated for 10 minutes at 37 kHz to ensure suspension. Alginate (100 ± 0.1 mg) was weighed out and added to the CNC solution, vortexed for 5 minutes, spun down to amalgamate the bio-ink and revortexed for 3 minutes. The resulting viscous solution was again spun down and sonicated for 10 minutes at 37 kHz. The solution was then sterilized with an autoclave at 121°C for a 20 minutes cycle to emulate the sterilization process that will be used for scaffolds for cells.

A 20 wt% GelMA solution was made by dissolving the GelMA in a 0.5 wt% LAP solution at 80°C. Then, 1 mL of the GelMA solution was added to the autoclaved alginate and CNC solution

after being filtered through a 0.22 μm syringe filter. The resulting bio-ink was then vortexed for 5 minutes to ensure thorough mixing of the two solutions resulting in 5 mL of bio-ink with 2 wt% alginate, 4 wt% GelMA and either 4 wt%, 5 wt% or 6 wt% CNCs.

Bio-inks consisting of 2 wt% alginate and 8 wt%, 9 wt% or 10 wt% GelMA were also produced to compare CNC containing bio-inks to ones with equivalent polymer concentrations and were denoted by their polymer concentrations (wt% alginate: wt% GelMa) For each bio-ink GelMA was dissolved in 5 mL 0.1 wt% LAP solution by heating at 80°C. Alginate was then added at 2 wt% (100 ± 0.1 mg) and allowed to be stirred overnight on an 80°C hotplate. Bio-inks were cooled to room temperature before rheological and mechanical characterization was completed.

2.2.3.2 – Rheometer

The bio-inks rheological characteristics were analyzed with a Bohlin-CS Rheometer with a cone-plate geometry (CP 4-40, 4° gap angle with 40 mm diameter). Constant rate mode was used to determine the steady shear viscosity versus shear rate curves at room temperature. The shear rate was swept up and down in order to show the bio-inks' ability to recover once shear stress was removed.

2.2.3.3 – Uniaxial compression

Samples for uniaxial compression were made using cylindrical PDMS molds with a diameter of 6 mm and heights ranging from of 0.5-1 mm. Bio-inks were added to the molds and subjected to three different conditions: UV irradiation for 10 minutes and then placed in 1xPBS buffer for >12 hours, 0.5 wt% $CaCl_2$ bath for >12 hours, or 10 minutes UV irradiation and then placed in 0.5 wt% calcium chloride for >12 hours.

Compression modulus was determined using a universal material tester (UMT) provided by Dr. Boxin Zhao from the University of Waterloo in the Department of Chemical Engineering. The UMT was configured with two parallel plates with one attached to a 42742410 kg force plate. Samples were placed on glass slides on the bottom plate and the top plate with the force plate was lowered unto the sample until 3.468 $x10^3$ Pa of force was registered at which point the top plate was paused for five seconds (s) to establish a baseline thickness of the sample. The top plate then continued to press down 0.3 mm over the course of 40 s and the force was measured every$7x10^{-3}$ s. The force and the deformation were converted to engineering stress and strain and the compression modulus was taken to be the slope of the stress strain curve for the first 10% of deformation. Three samples of each hydrogel were used to determine an average compression modulus.

2.2.3.4 Printing

All prints were completed on APTES treated #1.5 glass cover slips to ensure print adhesion throughout processing. Briefly, coverslips were submerged in 5:3 piranha solution (15.8 M nitric acid: 9.8M hydrogen peroxide) to remove any organic compounds and to activate the surface by converting silicon dioxide groups into silanol groups.[57] The glass cover slips were then rinsed twice in ultrapure water to remove excess piranha and placed in an ethanol solution consisting of 2 % (v/v) APTES for 12 hours. The treated coverslips were then sonicated twice in ethanol and once in ultrapure water to remove any excess APTES. They were dried under nitrogen stream and stored in a plastic petri-dish until needed.

Prints consisting of single filaments were completed using a FlashForge™ Creator Pro (FlashForge, China) fitted with Ultimus™ V high precision dispenser (Nordson EFD, USA). Bio-inks were centrifuged at 2000xg for 3 minutes to remove any air bubbles, placed in 10 mL

pneumatic syringes and centrifuged again. The pneumatic syringes of bio-inks were then placed into a custom printer head. A zig-zag pattern was designed and converted into g-code. Prints were made with 32-gauge (~100 μm diameter) nozzle operating at 12.5 mm/s and 276 kPa for the 2:4:6 bio-ink and 138 kPa for the 2:10 bio-ink.

Trench and cone patterns were first designed in Solidworks, converted into stereolithography (STL) files and uploaded to the Tissue Structure Information Modeling (TSIM) software. 3D prints were completed using a BioBot^{TM} Basic 3D printer (Advanced Solutions Life Sciences, USA) with 100 μm nozzle operating at 12.5 mm/s and a 276 kPa printing pressure for the 2:4:6 bio-ink and 138 kPa for the 2:8 bio-ink.

2.3 Results and Discussion

2.3.1 GelMA Characterization

From the H-NMR of the produced GelMA and the gelatin, a decrease in signal can be observed with the peak at 2.8 ppm (a). This peak is associated with the methylene protons of the unreacted lysine groups. The degree of substitution can be estimated through the normalization of the integral of the aromatic peaks at 7.2 ppm (e) and taking the ratio of the unreacted lysine groups in GelMA (I_{GelMA}) and the lysine groups in gelatin ($I_{Gelatin}$).[56]

$$DOS = 1 - \frac{I_{GelMa}}{I_{Gelatin}} = 1 - \left(\frac{0.1864}{0.7375}\right) = 0.7473 \quad (1)$$

Using a similar procedure Shirahama *et al.* were able to produce GelMA with over 96% DOS.[56] In their research they only reported the results of each reaction scenario once. Thus, they had not investigated batch to batch variation of GelMA. Four batches of GelMA were produced within the Tang lab and were characterized using H-NMR (appendix B). The average DOS for the four batches of GelMA was found to be 0.852 ± 0.084. The high standard deviation shows that

there is a large amount of inconsistency between batches of GelMA. The methacrylic anhydride is not miscible in water and therefore must be emulsified in the gelatin solution to react with the gelatin. This emulsification is done through the slow dropwise addition of methacrylic anhydride and high rates of stirring. If the speed of the stirring is reduced from one batch to the next, the size of the emulsified methacrylic anhydride droplets will be bigger resulting in less surface area readily available for the reaction. Similarly, if the rate at which methacrylic anhydride is added to the reaction vessel is increased the droplets of methacrylic anhydride can amalgamate together and reduce the surface area available for the reaction reducing the rate of reaction. The incorporation of standard stir rates and the use of a syringe pump to add methacrylic anhydride at a consistent rate should be implemented to reduce the batch to batch changes in the DOS.

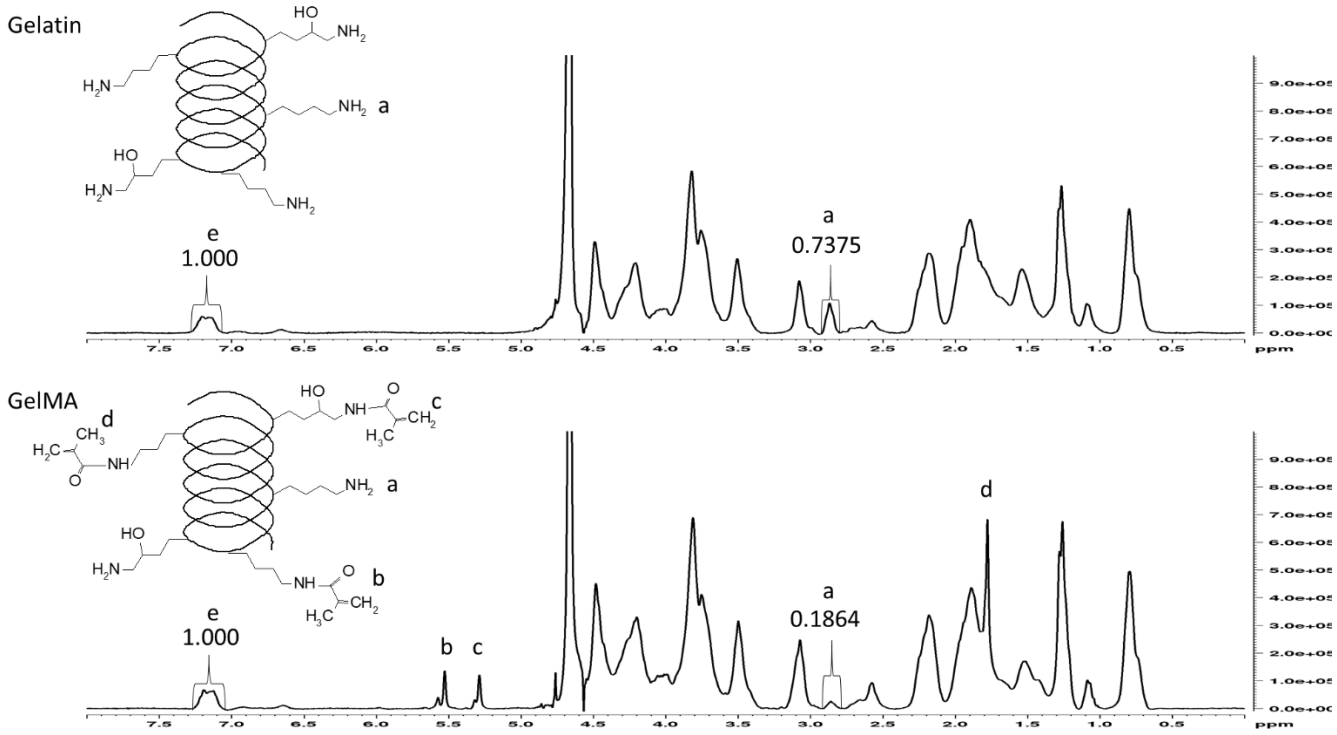

Figure 9: HNMR of gelatin and GelMA with peaks corresponding to (a) methylene protons of unreacted lysine groups,(b) acrylic protons of methacrylamide grafts of lysine groups and (c) hydroxyl lysine groups, (d) methyl protons of methacrylamide grafts and (e) aromatic protons. Degree of substitution of methacrylate anhydride unto lysine groups was determined by normalizing the above spectrums to the aromatic peaks (e) and comparing the integrals of the unreacted lysine groups (a).

2.3.2 Rheology of Bio-inks

Figure 10 shows the results of constant shear rate experiments performed on different bio-inks in which the viscosity was measured as the shear rate was increased. Bio-inks that contained CNC show shear-thinning properties across the entire ranges of shear rates. The viscosities of bio-inks without CNCs remain relatively constant at low shear (<10 s^{-1}) and begin to exhibit some shear thinning at higher shear rates (>10 s^{-1}). As previously mentioned, when CNC containing hydrogels are subjected to shear stress, the CNCs at the gel surface align themselves longitudinally in the direction of the shear stress. Consequently, the aligned CNCs begin slipping past each other resulting in an apparent decrease in viscosity.[49]

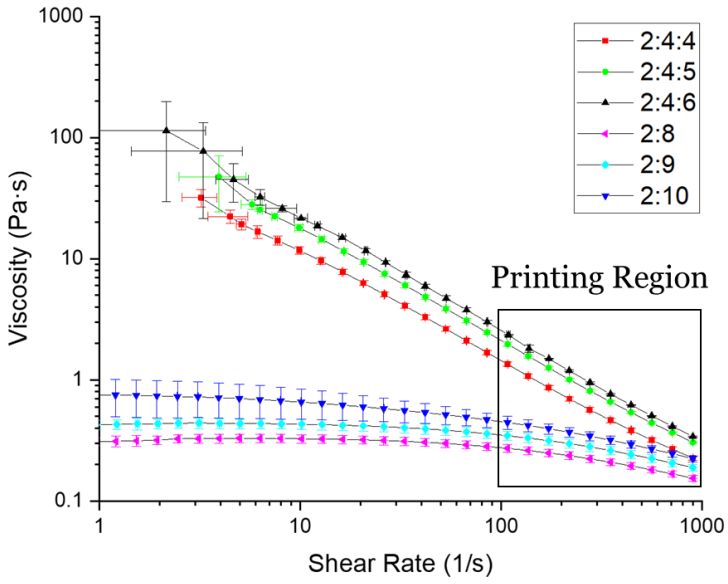

Figure 10:Viscosities of bio-inks subjected to increasing shear rates. Bio-inks containing CNCs show increased rates of shear thinning evident by the high viscosities at low shear rates (1 -10 s^{-1}) that drop to comparable viscosities in the printing region (100-1000s^{-1}) of the bio-inks that do not contain CNCs.

Bio-inks containing CNCs were fitted to the power law model (Equation 1.6) across all shear rates and the K and n values were determined.

Bio-inks with CNCs – All shear rates (1 to 1000 s^{-1})		
Bio-Ink	K [Pa·s^n]	n [Unitless]
2:4:4	90.421 ± 2.651	0.106± 0.006
2:4:5	138.135 ± 3.336	0.095 ± 0.004
2:4:6	188.756 ± 4.903	0.064 ± 0.004
Bio-inks without CNCs – Low shear rates (1 to 10 s^{-1})		
Bio-Ink	K [Pa·s^n]	n [Unitless]
2:8	0.316 ± 0.003	1.022 ± 0.006
2:9	0.436 ± 0.002	0.999 ± 0.004
2:10	0.769 ± 0.005	0.937 ± 0.004
Bio-inks without CNCs – High shear rates (100 to 1000 s^{-1})		
Bio-Ink	K [Pa·s^n]	n [Unitless]
2:8	1.010 ± 0.060	0.728 ± 0.010
2:9	1.404 ± 0.085	0.709 ± 0.010
2:10	2.232 ± 0.120	0.665 ± 0.009

Table 1:Fitted values for flow consistency index (k) and flow behaviour index (n). Bio-inks containing CNCs were fitted across all shear rates. Bio-inks that contained no CNCs were fitted at both high shear rate (100-1000 s^{-1}) and for low shear rates (1-10 s^{-1}).

Two different fitting were made for the bio-inks that did not contain CNCs. The first was done from 1 to 10 s^{-1} to find the K and n values at low shear rates. Viscosities at low shear rates were calculated using the fitted values for K and n, subbing them into the power law model (Equation 1.6) and setting the shear rate at 1 s^{-1}.

From previous research done in the Tang lab, the shear rate experienced by the hydrogels during printing was around 300 s^{-1}.[58] Using this as a reference point, the Power model (equation 1.6) was fitted for shear rates ranging from 100-1000 s^{-1} for the bio-inks that did not contain CNCs. The n values for high shear rates was used to determine the shear rate that would be experienced at the wall of the micro-extrusion nozzle with the Bruneaux et al. equation (Equation 1.10). These calculated shear rates were then re-entered into the power model (Equation 1.6) and into the Ostwal De Wael expression (Equation 1.5) to find the viscosity and the shear stress that cells would experience at the wall of the micro-nozzle, respectfully.

Figure 11a shows the viscosity of the static bio-inks. Figures 11 b and c show the printing viscosity and the shear stress experienced by the bio-ink at the wall of an extrusion nozzle during the printing process respectively.

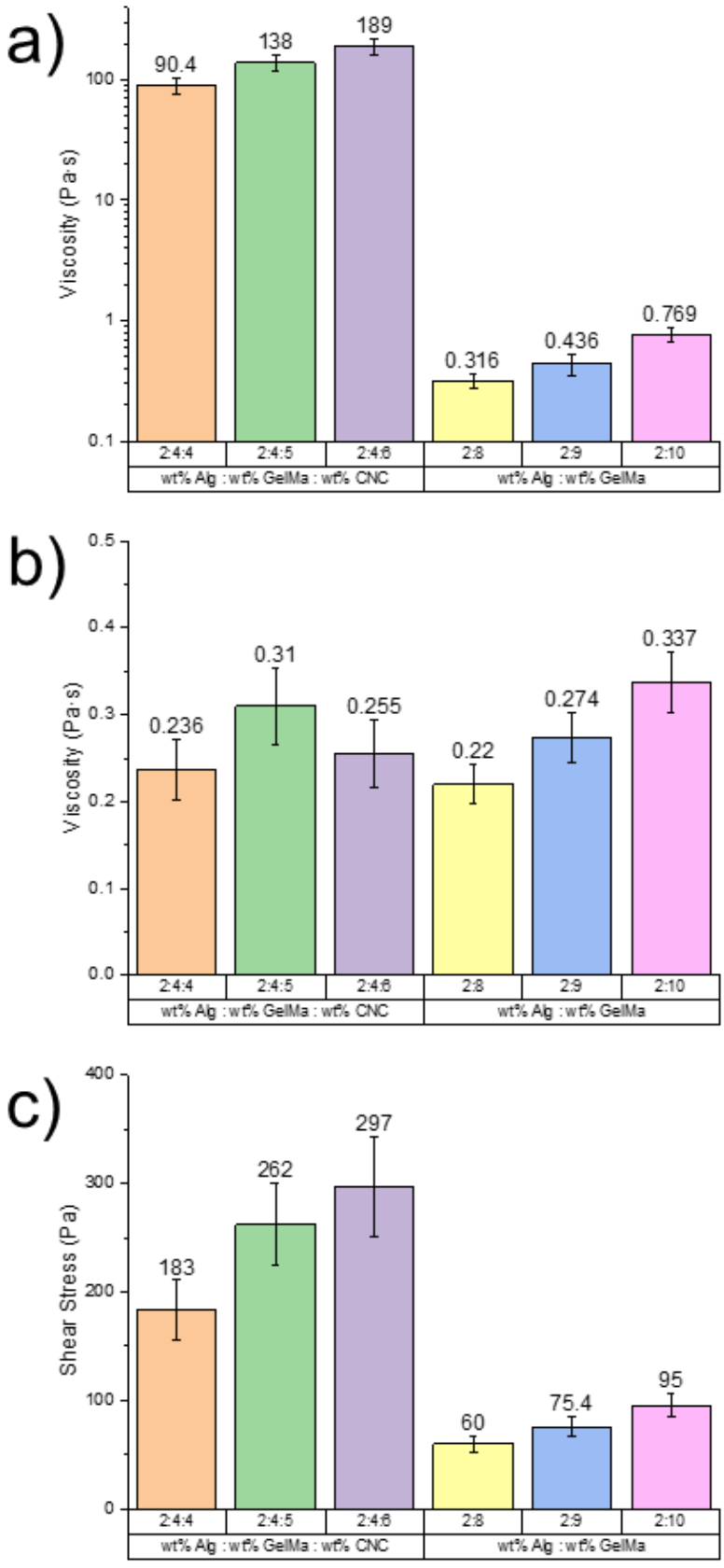

Figure 11: Calculated values for (a) static bio-ink viscosities, (b) viscosity and (c) shear stress at the wall of the extrusion nozzle during the printing process. Comparing static viscosities with printing viscosities shows that viscosities are 2-3 orders of magnitude greater for static viscosities but drop to comparable viscosities when printing which is ideal for printing as the higher static viscosity allows for greater shape retention after extrusion.

Comparing Figure 11a with Figure 11b a large difference in the viscosities of the CNC containing bio-inks can be observed. This difference in viscosity between the static bio-inks containing CNCs and those being printed is key for shape retention throughout the printing process. When the bio-ink is static the high viscosities prevent the bio-ink from flowing allowing it to retain the shape of the printed structures. In this case it is observed that the bio-inks viscosities during printing ranged from 0.220 to 0.337 Pa·s but when they are static the viscosities of the CNC containing bio-inks are much higher ranging from 90.4 to 189 Pa·s. On the other hand, the printed viscosities of the bio-inks that do not contain CNCs only slightly when compared to the static viscosities of the same bio-inks.

The 2:4:6 bio-ink experienced the highest shear stress at 296.9 Pa which is nearly a 5-fold increase from 60.0 Pa shear stress experienced by the 2:8 bio-ink. CNC containing bio-inks nearly tripled their shear stress when compared to bio-inks with the same polymer content. This increase in shear stress was likely due to the rigid nature of the CNCs. While the shear stress experienced by the cells at the nozzle increased with the addition of CNCs, these shear stresses were still relatively small compared to value reviewed in literature. In their paper looking at the effect of shear stress on the printing of human mesenchymal stem cells (MSC) Blaeser *et al.* found that there was little change to cell viability when cells were subjected to shear stresses below 3000 Pa.[59] This value is almost 10x the amount of shear stress calculated for the 2:4:6 bio-ink. This suggests this bio-ink can potentially be used for encapsulated cell bioprinting. Shear stress can affect cells differently depending on the type of cell. Thus, cell encapsulation studies using the 2:4:6 bio-ink should be completed to determine its feasibility for encapsulated cell bioprinting.

The viscosities calculated in Figure 11b (0.236 to 0.310 Pa·s) with the bio-ink containing CNCs were two to three orders of magnitude lower than the viscosities calculated for static bio-inks in Figure 11a. These differences in viscosity is beneficial for 3D bioprinting if there is little to no hysteresis observed in the bio-inks. To test the hysteresis of the 2:4:6 bio-ink, a constant shear-rate rheology measurement was taken for both increasing shear rates and decreasing shear rates. Figure 12 shows that there is very little hysteresis observed in the 2:4:6 bio-ink. This meant that the bio-ink recovered its viscosity once the shear rate was removed which suggests that the 2:4:6 bio-ink will be well suited for retaining its shape throughout the printing process

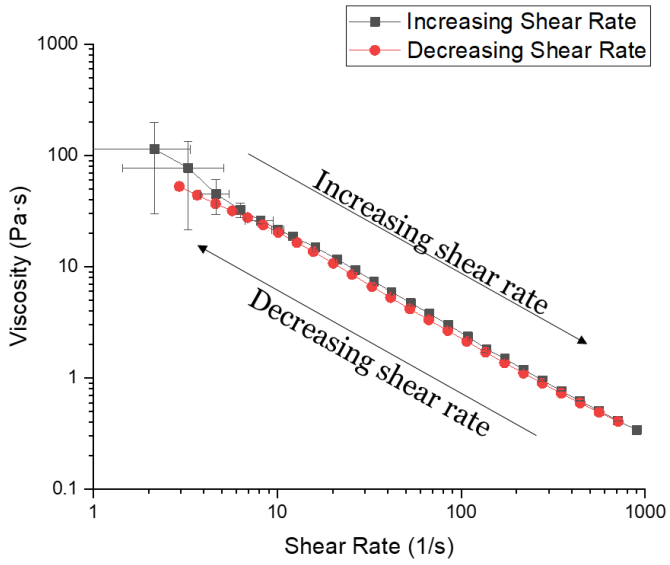

Figure 12: Viscosity vs shear rate of constant rate rheological measurements with both increasing and decreasing shear rates for 2:4:6 bio-ink. Little hysteresis observed between increasing and decreasing shear rates allowing for the instant recovery of viscosity after the bio-ink is extruded which increases the shape retention of prints throughout the printing process.

2.3.3 Uni-axial Compression

Looking at the data presented in figure 13 it is observed that as the CNC concentration increased, there was an increase in the compressive modulus in both the UV-treated and UV-$CaCl_2$ treated bio-inks. This increase in compressive strength is likely due to the formation of percolated networks of CNCs within the crosslinked bio-inks.

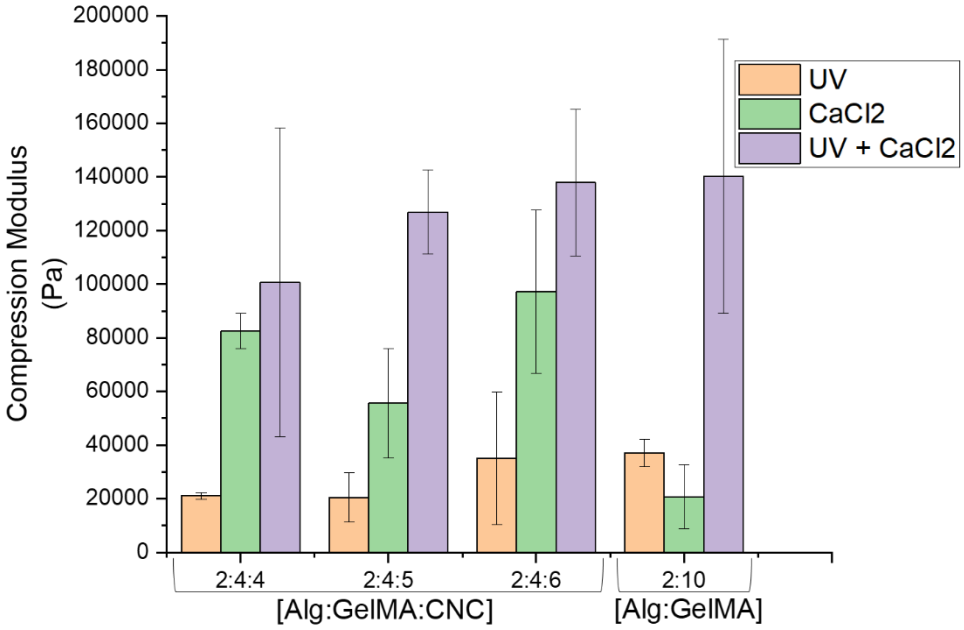

Figure 13:Compression modulus for bio-inks crosslinked through UV, $CaCl_2$ or UV+$CaCl_2$.

The trend of increasing compression modulus with the increasing CNC concentration was not observed in the bio-inks that were crosslinking with $CaCl_2$ only. Instead, a decrease in the compression modulus was observed when the CNC concentration was increased from 4 to 5 wt% followed by an increase in compression modulus as the CNC concentration increased from 5 to 6 wt%.

While not completely understood, it is speculated that the electrostatic interactions can explain the decrease in compression modulus observed as the CNC concentration increases from 4 to 5 wt%. Initially when CNCs are added to the bio-inks, the alginate and the gelatin will begin wrapping themselves around the CNCs increasing the strength of the hydrogels. As the concentration of CNCs increases past the point at which alginate and gelatin can wrap themselves around the CNCs, they begin to interfere with the divalent cation crosslinking due to the negative

charges found on their surface. The CNCs' negative charges compete with the alginate for the divalent cations, which decreases the alginate crosslinking density and weakens the hydrogel. Increasing the CNC concentration even more can also create a secondary network of rigid particles that are now trapped within the alginate polymer network increasing the compression modulus of the hydrogels.

Electrostatic interactions between the alginate and the CNCs may explain the decrease in compression modulus observed from the 2:4:6 bio-ink to the 2:10 bio-ink. Polymers tend to wrap around nanomaterials such as CNCs. The production of CNCs involves treatment with sulphuric acid which resulted in sulphate functionalization on the surface of the CNCs creating a negatively charged surface. The carboxylic functional groups on the alginate have an isoelectric point at pH 5.4. Thus, since the bio-inks are mixed in water and have a pH of approximately 7.2-7.4, these carboxylic groups are negatively charged. When the alginate wraps itself around the CNCs, the negative surface charge causes the alginate's carboxyl groups to face away from the CNC and increase the chances of crosslinking with the divalent ions. The combined effects of the CNC's surface charge and rigidity results in a stronger crosslinked bio-ink.

Comparing the 2:4:6 and the 2:10 bio-inks that were UV-$CaCl_2$ treated indicates that the compressive moduli are relatively similar. In this case it is likely that the increased GelMA content of the 2:10 bio-ink resulted in a higher crosslinking density resulting in smaller pore sizes that would allow for the transfer of energy throughout the crosslinked bio-ink. The rigid nature of the CNCs and the formation of a percolated network within the 2:4:6 bio-ink would supply the strength to the crosslinked bio-inks rather than the crosslinking density of the GelMA. There is also a possibility that the alginate and GelMa had wrapped themselves around the rigid CNCs resulting

in larger pore sizes to form. Porosity and pore size studies should be completed to confirm that this is what is causing the same compressive moduli to be observed.

There is a large amount of error in the data as can be seen by the size of the error bars in Figure 13 which brings into question if the trends mentioned above are occurring within this bio-ink system. In this research each bio-ink was mixed once, and three samples of each crosslinking condition was measured using the UMT. Looking at the resulting data (appendix C) a large difference in the slopes can be observed especially in the 2:4:6 and 2:8 bio-inks that were crosslinked with UV and $CaCl_2$. To confirm that the trends seen in the compression experiment is accurate, the experiment should be repeated at least two times and the resulting compressive moduli of the different treatments of each bio-ink should be compared determine the reproducibility.

2.3.4 Hydrogel Printability

The 2:4:6 bio-ink was chosen for printing since it possessed the highest viscosity at low shear rates, low hysteresis and high mechanical strength (as shown in Figures 10, 12 and 13). The zig-zag pattern was chosen to observe how individual filaments of the bio-ink would behave. The average width of the 2:4:6 bio-ink filament was found to be 309 ± 68 μm while the average width of the 2:10 bio-ink was found to be 474 ± 35 μm which is considerably larger than the 2:4:6. It can be explained by the high viscosity of the 2:4:6 bio-inks which prevents it from spreading after deposition. All the widths of the printed filaments were larger than the nozzle diameter (100 μm). Gravity acting on the filaments can cause them to expand outwards resulting in them losing their initial shape. In addition, the APTES treated slides can also influence the spreading of the bio-inks. APTES helps the crosslinking between the printed scaffolds and the glass slip but by adding APTES to the surface of the glass it becomes more hydrophilic. This decreases the contact angles

and thus the filaments on the glass spread out. This phenomenon means that changes in the design of the printed structures needed to be adjusted depending on the surface in which they were printed on.

The printed cone structures and the trench structures are shown in Figure 14. In both cases, the 2:4:6 bio-ink was able to maintain its relative shape throughout the printing process while the 2:10 bio-inks structures collapsed. Even though the 2:4:6 bio-inks structures maintained their structures, there were evidences of gravitational effects mainly in the rounding of the tops of the trenches and the bending of the cones. Since the printing time for each print is on the order of minutes there was plenty of time for them to start to collapse on themselves before they could be crosslinked.

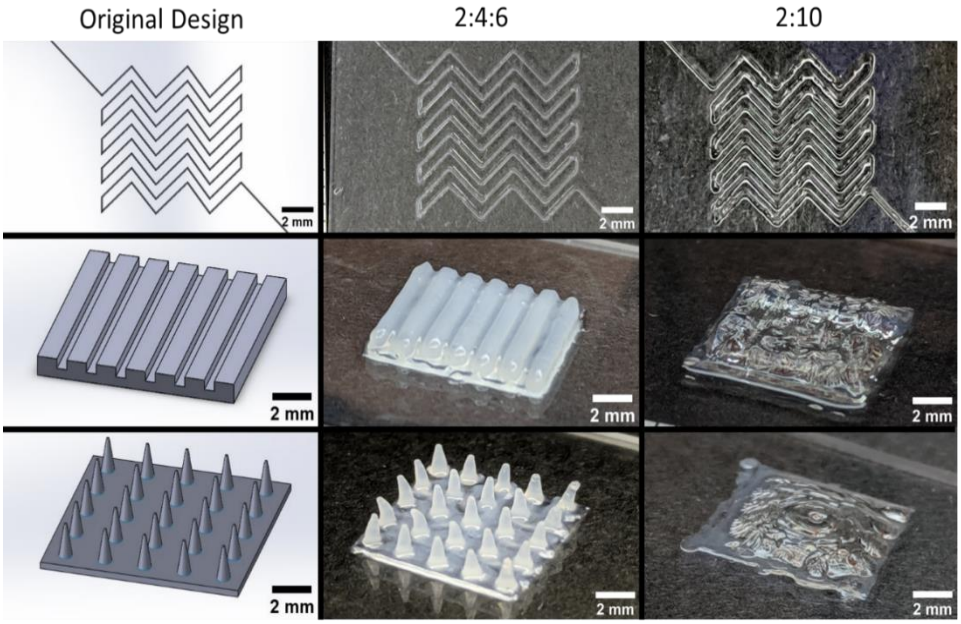

Figure 14: Comparison of 2:4:6 and 2:10 bio-ink printability.

One way to help reduce the gravitational effect would be to incorporate a UV lamp into the printer so that the printed filaments can be crosslinked once being extruded. This would help to solidify the filaments and maintain the printed structure throughout the printing process. Ouyang *et al.* developed a process for bioprinting that uses a clear nozzle and a UV light in order to crosslink methacrylate hyaluronate as it is being extruded from the pneumatic syringe.

This allowed them to produce high fidelity structures with less viscous bio-inks.[60] The issue with this method is the long exposure time to the UV radiation which will affect the cell viability in cell-embedded systems.[61]

One way to mitigate the use of UV radiation is to change the photo-initiator to one that works in the visible spectrum. Lim *et al.* demonstrated that high fidelity prints with GelMA can be achieved using a ruthenium and sodium persulfate (RU/SPS) co-initiator system and a 400-450 nm light source. They compared this system with the conventional Irgacure 2959 and found that while it might take longer for the RU/SPS system to fully crosslink, it was less cytotoxic and cell viabilities were over 85%.[62]

2.4 Conclusion and Future Work

The GelMA used in this experiment had a DOS of 74.7% which was lower than the reported DOS for this procedure. This could be caused by the high variability in the reaction conditions as multiple batches of GelMA have been produced with a wide range of DOS. Therefore, care in replicating the reaction conditions exactly must be taken to minimize the batch to batch changes in the GelMA.

The rheometry of the bio-inks shows that the 2:4:6 bio-ink had the highest viscosity across all the shear rates, exhibited a high degree of shear thinning and the ability to recover its viscosity once shear rates were reduced. In the bioprinting region, it was found to have a viscosity of 0.319 Pas and the shear stress at the wall was found to be 296.9 Pa. Cell viability studies will need to be carried out to determine whether the 2:4:6 bio-ink is compatible with embedded cell bioprinting.

There was no significant difference in the compressive strength of the 2:4:6 bio-ink and the 2:10 bio-ink when crosslinked with UV and $CaCl_2$. This is attributed to the increased GelMA concentration of the 2:10 bio-ink which likely produced smaller pore sizes increasing the polymer networks ability to transfer energy across the whole structure while the 2:4:6 bio-ink relies on the rigidity of the CNCs to increase its strength. Since pore size could impact cell proliferation, future studies into scaffold porosity and pore size should therefore be done.

The 2:4:6 bio-ink was found to produce higher fidelity prints when compared with the polymer concentration equivalent 2:10 bio-ink. This was mostly attributed to the bio-inks ability to recover its viscosity when the shear stress was removed. The fidelity of the printed scaffolds was influenced by long printing time and the gravitational forces. Methods to decrease the deformation of the printed architecture were discussed as well.

Chapter 3: Evaluation of Bio-ink to Produce Simple Extravasation Models

3.1 Introduction

As the prevalence of CRC increases so does the need for more research in how to treat it. Metastasis formation is the primary cause of death in CRC.[11] The metastasis cascade is a complicated multistep process that is continuously being studied in the hope of finding treatments to prevent the spread of CRC to different organ systems. The extravasation step of metastasis occurs when circulating tumour cells stick to the inner surface of the blood vessels and transverse through the endothelial cell layer. Models currently used for extravasation studies either use a filter membrane to simulate the endothelial cell layer or operate in an avian xenograft microenvironment which can affect endocrinological factors crucial to cancer cell viability.[12] Ideally, the extravasation model would consist of a human endothelial cell layer that acts as a barrier for the traversing of circulating tumour cells and could be placed in a device to allow the circulating of blood to better mimic the blood vessels.

While a complete extravasation model is well out of the scope of this thesis, this study looks at the use of 2:4:6 bio-ink in creating cell scaffolds to support the growth of an endothelial monolayer using the hybrid cell line EA-hy 926 to mimic the conditions found in human blood vessels. Factors effecting cell adhesion to the scaffolds are discussed and suggestions for modifications to the scaffolds are made. HCT 116 cells were seeded unto the scaffolds after EA-hy 926 cells to mimic circulating tumour cells resulting in a discussion on the fluorescent staining and tracking of HCT 116 cells.

3.2 Materials and Methods

3.2.1 Materials

GelMA made from 300 bloom type A gelatin with 92% degree of substitution was provided by Yun Wu, Department of Chemistry University of Waterloo. Pharmaceutical grad sodium alginate (PROTANAL LF 10/60FT) was provided by the FMC corporation. CNCs hydrolyzed from wood were provided by Dr. Michael Tam from the Department of Chemical Engineering at the University of Waterloo. Lonza's Dulbecco's modified eagles medium (DMEM, 12-604F) with 4.5 g glucose and with L-Glutamine along with GIBCO 100 mM sodium pyruvate (11360), 0.025% trypsin-0.01% ethylenediaminetetraacetic acid solution (TRY/EDTA, R001100), 0.4% Trypan Blue (15250061), LIVE/DEAD™ viability/cytotoxicity kit (L3224), Invitrogen™ Qtracker™ 655 cell labeling kit and CULTREX 0.01 wt% poly(L-lysine) solution (70 000 – 150 000 kDa, 343810001) was purchased from ThermoFisher. Fetal bovine solution (FBS, 97608) was purchased from VWR. OmniPur® 10X phosphate buffered saline concentrate (10xPBS) (6506-1L), $CaCl_2$ (C1016), LAP (900889) was purchased from Sigma-Aldrich.

3.2.2 Bio-ink Mixing

A bio-ink consisting of 2 wt% alginate, 4 wt% GelMA and 6 wt% CNC was mixed in the same method as previously mentioned in Section 2.2 with some modifications. To aid the filtration of GelMA, the CNC was initially mixed in 3 mL ultrapure water instead of 4 mL ultrapure water. The subsequent mixing steps were completed as reported until the addition of LAP photo-initiator and GelMA. LAP was dissolved with ultrapure water to form a 0.25 wt% solution. GelMA was dissolved in the LAP solution at 100 mg/mL and 80°C. Two millilitres were added to the CNC/Alginate mixture to form the 2:4:6 bio-ink with 0.1 wt% LAP.

3.2.3 Scaffold Printing

Scaffolds were made using the modified FlashForge™ Creator Pro printer fitted with the Ultimus™V high precision dispenser. Printing was conducted with a 32-gauge microfluidic nozzle (~100 μm diameter) at 12.5 mm/s with a pneumatic pressure of 276 kPa on APTES treated slides. Once printed scaffolds were imaged and physically crosslinked with 1 mL of 0.5 wt% $CaCl_2$ solution for 1 minutes. Scaffolds were further crosslinked under UV for 10 minutes and stored in 3 mL 0.5 wt% $CaCl_2$ solution overnight. Before seeding, the scaffolds were placed under a UV germicidal lamp for 30 minutes to eliminate contamination that may have occurred during the printing process.

3.2.4 Cell Seeding

The endothelial somatic cell line EA-hy926 cells (passage 12) was harvested using TRY/EDTA and incubated for five minutes at 37°C and 5% CO_2. Detached cells were washed with 1xPBS and counted using trypan blue and a hemocytometer. The cell suspension was then centrifuged for 3 minutes at 400 xg to form a cell pellet and resuspended with complete cell media (DMEM + 10% FBS) at a concentration of $3.25x10^6$ cells/mL. The scaffolds were removed from the $CaCl_2$ solutions and 20μL of the cell suspension ($6.5x10^5$ cells) was seeded on top of the scaffolds. Seeded scaffolds were then incubated at 37°C and 5% CO_2 for four hours before 3 mL of complete cell media was added and placed back into the incubator for 24 hours. Single scaffolds were imaged on day one and three to see if a monolayer of cells had developed. A second seeding of 65 000 EA-hy 926 cells was done on day three and scaffolds were imaged on days four and six.

On day six human colorectal tumour cells (HCT 116, Passage 48) were harvested with TRY/EDTA solution and were counted using trypan blue and a hemocytometer. These cells were then centrifuged at 400 xg for three minutes to form a cell pellet and resuspended in complete cell medium (DMEM with 10% FBS and 1mM sodium pyruvate) at $1x10^7$ cells/mL. HCT 116 cells

were labelled with Qtracker™ 655 cell labeling kits protocol. Briefly, a 10 nM solution of Qtracker™ nanocrystals was prepared by mixing 1 µL of the supplied 2 µM in 50 mM borate buffer solution with 1 µL of carrier buffer (1xPBS pH 7.2) in 200 µL of complete cell medium before $1x10^6$ cells (100 µL) were added. Cells were incubated for one hour at 37°C and 5% CO_2 before being centrifuged and resuspended in complete cell media three times to remove excess Qtracker™. The cells were diluted to $0.5x10^6$ cells/mL with complete cell media and 20 µL was seeded on top of the scaffolds (10 000 cells) and allowed to incubate for four hours at 37 °C and 5% CO_2 before additional cell media was added. Cells were then imaged after 24 hours.

3.2.5 Lysine Treated Scaffolds

Scaffolds treated with poly(L-lysine) were created in the same manner as previously mentioned in Section 3.2.3 but were printed with the BioBot™ bioprinter in place of the FlashForge™ modified 3D printer. Once sterilized under the UV germicidal lamp the scaffolds were covered with 2 mL 0.01 wt% poly(L-lysine) for 24 hours at room temperature before being rinsed with 1xPBS three times to remove excess poly(L-lysine). Treated scaffolds were seeded by the addition of 2 mL of $1.0x10^6$ cell/mL cell suspension to the wells containing the scaffolds.

3.2.6 Scaffold Imaging

Imaging of seeded scaffolds was done using a Zeiss LSM 700 confocal microscope (Carl Zeiss AG, Germany) z-stack function. The EA-hy926 cells were stained using an INVITROGEN™ LIVE/DEAD™ Viability/Cytotoxicity kit, for mammalian cells (ThermoFisher, L3224). Briefly, 0.5 µL of the supplied 4 mM calcein in DMSO was dissolved in 2000 µL of 1xPBS (pH 7.2) along with 2 µL of the 2 mM ethidium homodimer-1 (ETHD-1) to make a 1 nM calcein-AM and 2nM ETHD-1 dye solution. Cell scaffolds were rinsed with 3 mL 1xPBS three times to remove any non-adherent cells and incubated for 30 minutes at 37°C, 5% CO2 in the dye

solution. Before imaging the scaffolds were rinsed again with 3 mL 1xPBS three times to remove any excess dye.

3.3 Results and Discussion

The scaffold was designed with two distinct sections. The first section is the “villi” section which consists of cones extruding out of a flat layer bio-ink. This section was designed to show the ability of the hydrogel to maintain its shape through the printing process and to see if EA-hy 926 cells would be able to proliferate up the surface of the structure. The final section was the “trench” section and was designed to mimic half a blood vessel. This is designed to be used in a simple model of the extravasation process that occurs in the metastasis cascade.

ETHD-1 is a high-affinity nucleic acid stain that is used to stain dead cells whose membranes have become compromised allowing the dye to have access to the nucleic acids within the cells. When bound to nucleic acids, it emits a strong red fluorescent signal but still emits a weak signal when not bound to nucleic acids. The amino groups found in its structure induce a positive charge at physiological pH which causes it to have a high affinity to the negatively charged alginate and CNCs within the bio-ink. This allowed for the imaging of the scaffold structures without the need for extra dyes.

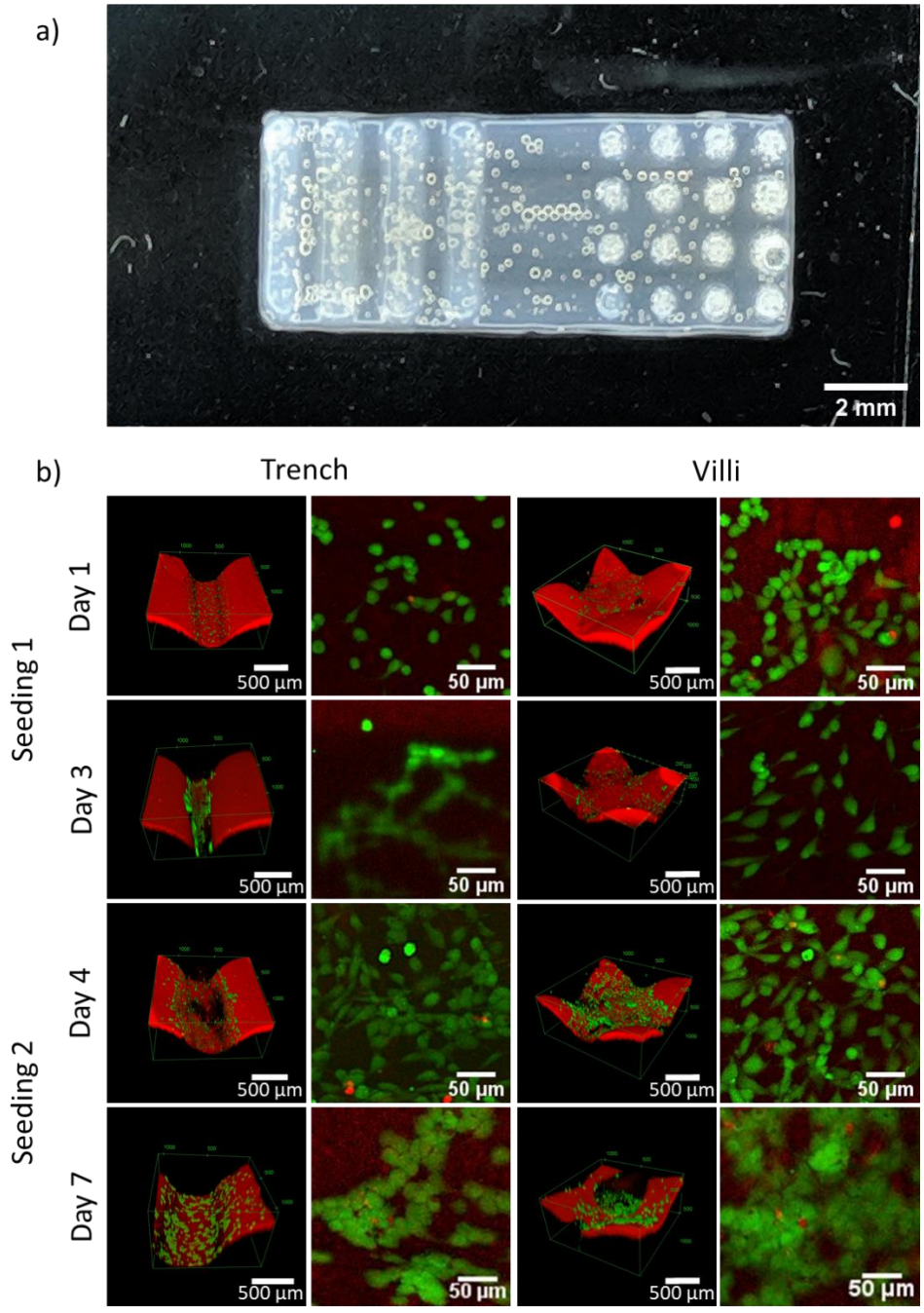

Figure 15:(a) 2:4:6 bio-ink scaffold printed using BioBot™ bioprinter. (b) 3D rendered images and zoomed in section of confocal z-stacks for 2:4:6 bio-ink scaffolds seeded with EA-hy 926 cells. A second seeding was done on day three to increase cell confluency. HCT 116 cells treated with Qtracker™ were seeded on day six but no fluorescent signal was observed.

To mimic the layer of endothelial cells that line the inside of blood vessels, EA-hy 926 cells were seeded at a density equivalent to that needed to seed a 2D culture with the same surface area and images were taken after 24 hours. Figure 15 shows cells were found on the surface of the hydrogel, both the trench and villi section. After 3 days of incubation, there was an increase in the number of cells at the bottom of the trench and villi structures. These cells are in areas that would have protected them from being washed away when additional cell media was added.

A second seeding EA-hy 926 cells on the scaffolds was attempted to see if more coverage of the scaffold was possible. The day four section of Figure 15 shows that a higher percentage of the scaffold was indeed covered after 24 hours from the second seeding, but a mono-layer of cells had not been formed. The cells were left for two more days to see if they would proliferate more as time went on. From the day seven section of Figure 15, it is evident that the cells are attaching to the surface of the scaffolds, but a complete monolayer is not observed.

The addition of GelMA was designed to allow the cells to attach to the scaffolds but it appeared that the cells did not have the opportunity to attach to the surface. One possibility is that the electrostatic repulsion between the cells and the scaffold surface prevented the cells from attaching to the surface. Heparan sulphate proteoglycans (HSPG) are a negatively charged polymer that is found in abundance on the surface of the cellular membrane giving the cell membrane an overall negative charge. HSPGs also play an important role in the binding of cells to extracellular membrane components and are highly susceptible to electrostatic interactions due to the large number of sulphate groups found on them.[63] Alginate and CNCs are both electronegative. The carboxylic functional groups found in alginates co-monomers β-D-mannuronic acid and (1-4) α-L-guluronic acid are negatively charged at physiological pH giving alginate an overall negative charge. The use of sulphuric acid in the production of CNCs results in many sulfate ester groups

($-OSO_3^-$) being added to the surface of the CNCs.[46] Again, these are negatively charged at physiological pH. This results in a scaffold with a highly electro negative surface that would repel the electronegative cell membrane preventing the cells from adhering to the cell binding sites found in GelMA and being washed away.

While the electrostatic repulsion prevented the cells from forming a complete mono-layer on the surface of the scaffolds, the cells were still able to attach to the surface of the scaffolds. This suggests that over time the cells can overcome the electrostatic repulsion and eventually attach to the cell binding sites that GelMA provides. In 2D cultures the cells do not have to overcome this electrostatic repulsion to attach and therefore fewer cells would need to be used to seed the surface of the culture. Future cell studies using the 2:4:6 bio-ink should therefore use higher cell densities for seed to increase the probability that the cells will attach to the surface of the scaffolds.

Even though a monolayer of EA-hy 926 cells was not achieved, HCT 116 cells were seeded onto the scaffolds without poly(L-lysine) with 10 000 cells in 20 μL of complete cell media plus 1 mM sodium pyruvate. These cells were treated with Qtracker™ to image them separately from the EA-hy 926 cells as the LIVE/DEAD™ only distinguishes between alive and dead cells and not different cell types. After 24 hours, no HCT 116 cells were distinguishable on the surface as can be seen in day seven of Figure 15. To determine whether the cells had not attached to the surface and had been washed away, the ability of Qtracker™ 655 to stain HCT 116 cells was investigated through recreation of the Qtracker™ staining protocol. When imaged with a confocal microscope, it was found that HCT 116 cells produced no fluorescence signal. Qtracker™ uses a β-amino acid analogue of Tat 47-57 which is a protein created by human immunodeficient virus that is permeable through the cell membrane. Since different cell types may take longer for the peptide to cross the membrane, the HCT 116 cells, may have not had long enough time to uptake the

quantum dots that are conjugated to the β-amino acid analogue. Therefore, to image HCT 116 cells on the scaffold, studies should be done to optimize the up take of quantum dots by the HCT 116 cells. Alternatively, another fluorescent cell tracker that uses a different mechanism of producing fluorescence should be investigated.

Poly(L-lysine) treatment of the scaffolds was done to see if it could help facilitate cell adhesion. Poly(L-lysine) is a polymer that contains a large concentration of positively charged amino groups and is used as a coating in culture plates to help cells overcome electrostatic forces associated with the materials used in cell culture plates. Figure 16 and Figure 17 shows how the treatment of the scaffolds with poly(L-lysine) effected the cell adhesion to the scaffolds. After 24 hours the cells appeared to be better distributed across the surface of the scaffold. This is evident by the increased number of cells that were observed on the tops of both the villi and the trenches.

The cells morphology was also different compared to the scaffolds not treated with poly(L-lysine). The scaffolds that had been treated with poly(L-lysine) appeared to have more elongated cells which was associated with a decrease in cell adhesion while fewer elongated cells were observed on the surface of scaffolds that had not been treated with poly(L-lysine). A possibly explanation for the increased number of elongated cells is in the poly(L-lysine) treated scaffolds is as the scaffolds are incubated within the cell media positively charged molecules start competing with the poly(L-lysine). Over time this could cause the poly(L-lysine) to detach from the surface of the scaffolds causing the cell to detach from the surface resulting in the elongation of the cells.

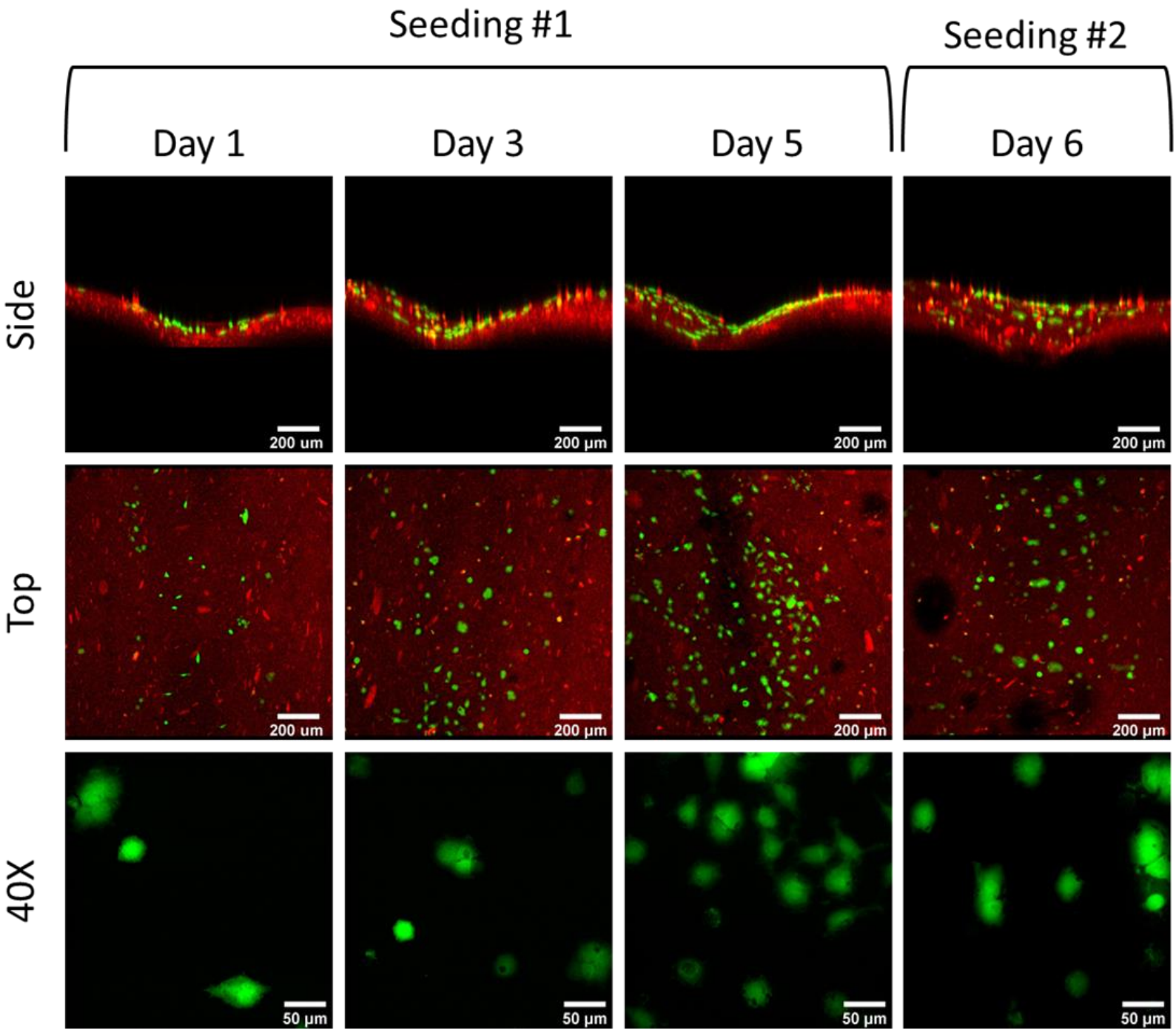

Figure 16: Trench section of scaffolds that were treated with poly-L-lysine and seeded with Ea-hy 926 cells. Increased confluency is observed for the first five days. Decreased confluency after the second seeding most likely caused deformations during the printing process and the degradation of the scaffold. Black spots in top down image are likely caused by collapse of bubbles from the printing process which suggest the degradation of the scaffolds.

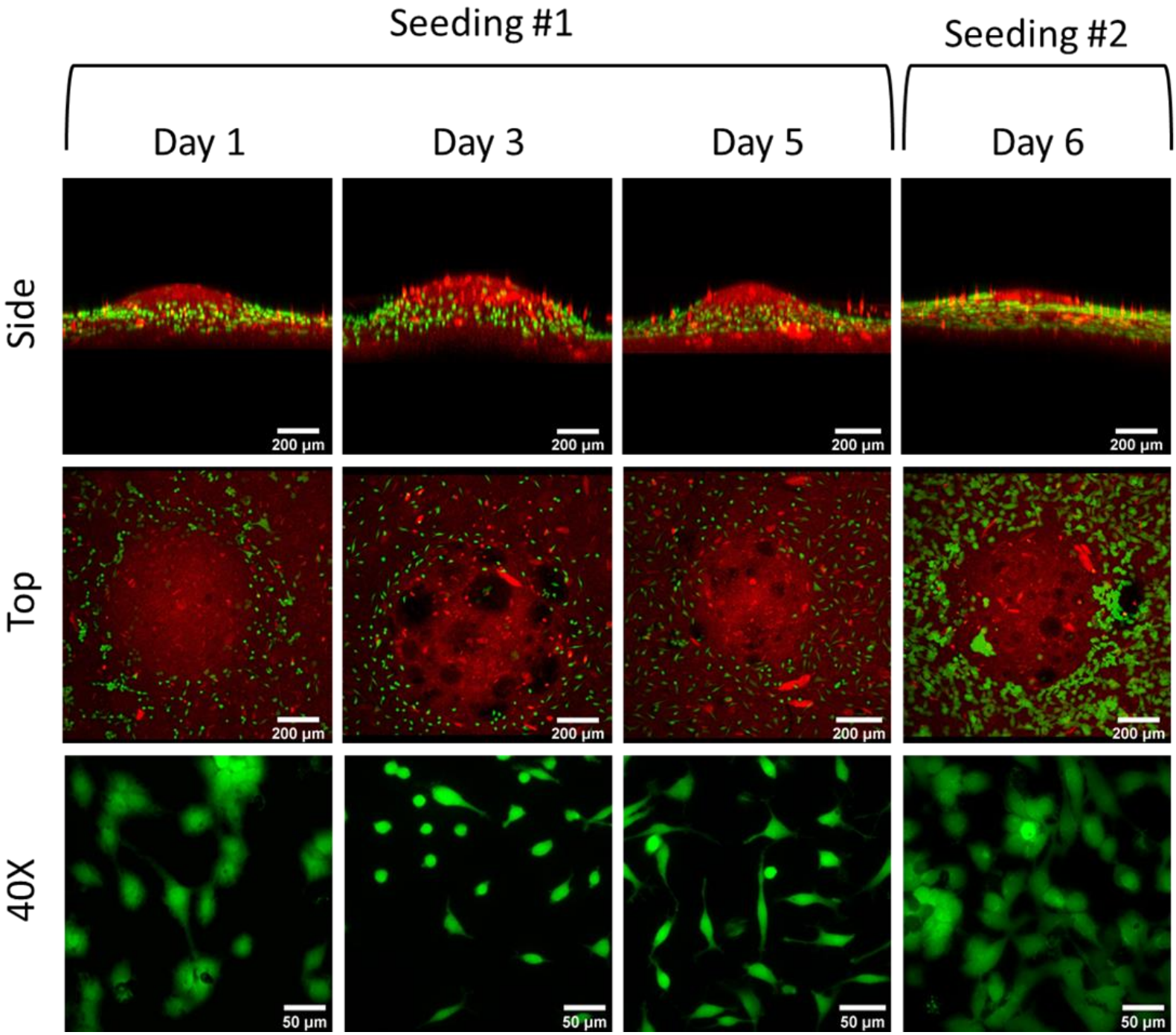

Figure 17: Villi section of scaffolds that were treated with poly(L-lysine) and seeded with Ea-hy 926 cells. Increased confluency and cell proliferation is observed after six days and two seedings of cells. Increased number of elongated cells most likely caused by the poly(L-lysine) detaching from the surface reducing cell adhesion to scaffold surface.

Looking at the trenches after the second seeding on day 6 showed a decrease in the cell confluency that was not observed in the villi structures. One possible explanation for this is that the shape of the trench appeared to flatter than the trenches imaged at earlier dates. This is an artifact of the printing process which would cause the cells to be more exposed and less likely to attach to the surface. Another possibility is that the surface of the scaffold is starting to degrade. Looking at Figure 17 on day 6 large dark spaces can be observed in the top view. These dark spaces are associated with bubbles that are formed during the printing process that have collapsed on themselves. The collapse of the bubbles could suggest that the scaffold is starting to degrade and that cells could be detaching decreasing the confluency of the cells.

While the poly(L-lysine) showed some improvement in the distribution of cells across the scaffolds, it was not enough to overcome the electrostatic repulsion between negatively charged cell membranes and scaffolds. This study used a 0.01 wt% solutions of poly(L-lysine) concentration and incubated the scaffolds for 24 hours. This low concentration may not have been high enough to effectively decrease the electrostatic charge of the scaffolds. Further research is needed to determine if higher concentrations of poly(L-lysine) or incubation times will reduce the electrostatic repulsion enough to promote cell proliferation.

Another possible method to decrease the electrostatic repulsion is to decrease the number of sulfate ester groups found on the CNCs. Lin *et al.* were able to produce CNCs from native cotton fibres with varying degree of sulfate ester groups by treating the sulphuric acid hydrolyzed CNCs with sodium hydroxide solutions ranging from 0.5 mol/L to 2 mol/L for one to three hours.

Reducing the number of sulfate ester groups on the surface of the CNCs will reduce the amount of electrostatic repulsion experienced by the cell. The issue with this approach is that the concentration of the sulfate ester groups may influence the structure and rheological properties of the CNCs. Their presence on the surface of the CNCs induces the formation of a negative electrostatic layer which promotes their dispersion in solvents such as water through electrostatic repulsion.[46] The removal of the sulfate ester groups could cause the CNCs to clump together and change their interactions with the alginate and GelMA. Future studies involving CNCs with different levels of sulfate ester groups should be completed to measure the changes in mechanical and rheological properties and to see if cell adhesion is enhanced.

While a mono-layer of cells was not achieved, the possibility remains that this bio-ink could be used for micropatterning of cells. Since the cells are less likely to adhere to the 2:4:6 bio-ink structures that are raised, patterns of cells could be formed using the valleys within the structures. The bio-ink could also be used as a natural masking agent for cell patterning. Printing the 2:4:6 bio-ink in the negative space of a pattern and seeding a desired cell line on top would cause the cells to grow in the positive space of the pattern with very few growing in the negative space. By removing the UV-crosslinking step and the photo-initiator, the 2:4:6 bio-ink would be eroded quickly through simple incubation in PBS as divalent ions are leached out of the structure and the alginate is no longer is crosslinked. This would leave cultures with cells patterned in the desired effect. Further research will need to be done to determine the scope for the usage of this bio-ink for micropatterning.

3.4 Conclusions and Future Work

The 2:4:6 bio-ink was used to create a cell scaffold with two different macrostructures and EA-hy 926 cells were seeded on top of the scaffolds. After 24 hours cells were observed on both structures as they had features that would protect cells during the addition of cell media or washing steps used in staining processes. Cell densities increased for both structures over the course of two days and a second round of cell seeding was introduced to increase the cell density. Three days after the second seeding a complete monolayer did not form. The inability of the cells to form a complete monolayer is thought to be caused by electrostatic repulsion between the negatively charged cell membrane and the negatively charged alginate and CNCs in the scaffolds.

Scaffolds treated with poly(L-lysine) were produced and cells were seeded on top for three days. Elongated morphologies of the EA-hy 926 cells on the scaffolds suggest that the cells that did attach had better attachment to the scaffold but the lack of cell confluency over the course of three days is again thought to be caused by the electrostatic repulsion seen in non-poly(L-lysine) scaffolds. The concentration of poly(L-lysine) used may have been too low or the incubation period may be too short to properly mitigate the electrostatic repulsion making it necessary for future studies using higher concentrations or longer incubation times. Another method to reduce the electrostatic repulsion would be to remove sulfate ester groups on the surface of the CNCs but would require additional research into the effect it would have on the rheological and mechanical properties of the bio-inks.

While a complete mono-layer was not attained the 2:4:6 bio-ink was able to support cell growth and cell proliferation. The electrostatic repulsion between the cell membrane and the bio-ink remains to be a hurdle but can potentially be overcome through studies using higher cell

seeding densities or increased concentrations of poly(L-lysine). Further research is needed to be done to determine if the 2:4:6 bio-ink is a viable option to produce extravasation models.

The 2:4:6 bio-ink could potentially be used for cell micropatterning through the removal of the UV-crosslinking step. It is speculated that the bio-ink could be used as masking agent that would allow patterning of cell where it is not applied and be removed through simple incubation in 1xPBS buffer. Future studies will need to be carried out to determine the bio-inks abilities to be used for cell micropatterning.

Chapter 4: Summary and Future Work

The metastasis of CRC to other organs is the number one cause of fatalities in CRC patients.[6] The extravasation process of the metastasis cascade is crucial for the spread of CRC. Current models used for researching the extravasation step either do not accurately represent the physiological local microenvironment or utilize the avian xenograft microenvironment.[12] 3D bioprinting is become an attractive method to produce models of the extravasation metastasis step that more closely mimic what is seen in the human body. This thesis aims at designing optimal bio-inks to produce biomimetic CRC extravasation models.

Working off previous work done in the Tang lab, Chapter 2 investigated the incorporation of GelMa into an alginate and CNC bio-inks in order to add cell binding sites to the system. By comparing the rheological and mechanical characteristic of different bio-ink formulations, a bio-ink consisting of 2 wt% alginate, 4 wt% GelMA and 6 wt% CNC was chosen for printability test. The bio-ink's high amount of shear-thinning and low hysteresis in viscosity recovery made it an ideal candidate for producing high fidelity patterns. Printability tests were completed and the 2:4:6 bio-ink was found to produce high fidelity patterns especially when compared to the polymer equivalent bio-ink 2:10.

Using the 2 wt% alginate, 4 wt% GelMA and 6 wt% bio-ink, Chapter 3 described the printing of cell scaffolds and the growth of a monolayer of EA-hy 926 cells to mimic the endothelial cell layer found in a human blood vessel. After 6 days and two cell seedings, the bio-ink was unable to support the growth of a complete monolayer of cells. It was concluded that this was caused by electrostatic repulsions between the negatively charged cell membranes and the negatively charged bio-ink. Subsequently, cell scaffolds were treated with poly(L-lysine) and changes in cell morphology were observed but the scaffolds were still unable to produce a

complete cell monolayer. While a complete cell monolayer was not achieved the cells were still able to attach and proliferate on the hydrogel suggesting that future steps may be taken to produce a complete cell monolayer.

Based on the study of the production of hybrid bio-inks for the development of biomimetic structures described in this thesis, the following recommendations for future work are made.

1) The production of GelMA can vary from batch to batch resulting in major shifts in the DOS of methacrylic anhydride to the lysine groups found on the gelatin. It is thought that these changes are a result of differences in the speed of stirring and the rate of addition of methacrylic anhydride into the reaction vessel. By standardizing the speed of the stir bar and the use of a syringe pump to add the methacrylic anhydride, the batch to batch variation of GelMA can be avoided.
2) From calculations of the shear stress on the wall of an extrusion nozzle, the 2:4:6 bio-ink was found to have a much lower shear stress than that used in literature. While this would suggest that the 2:4:6 bio-ink would be suited for cell encapsulation, future studies involving cell encapsulation must be completed to confirm that this is the case.
3) The error bars observed in the uni-axial compression tests are relatively large and thus are not reliable for data analysis. The size of the error bars is caused by the lack of replicates in the experiment. To reduce the error bars, the experiment should be completed with each bio-ink being mixed three times and three samples of each crosslinking condition being measured with the UMT. This increase from N=3 to an N=9 samples should reduce the size of the error bars and allow for more confidence in the conclusion drawn from the data.

4) While the 2:4:6 bio-ink was able to maintain its shape better than the polymer concentration equivalent 2:10 bio-ink, slight deformation caused by gravity was still observed. During the current printing process, the bio-ink's ability to retain their shape is due to its ability to return to its original viscosity after shear stress is removed. The bio-ink has not been crosslinked and is therefore susceptible to flow overtime. The addition of UV crosslinking light to the printer head would improve the shape fidelity as the ink would begin solidifying as soon as it is printed. This method would be useful for printing scaffolds without cells but could cause a decrease in the cell viability when used for cell embedded printing. Different photo-crosslinker systems that are not cytotoxic and do not use UV light should be investigated for use with the 2:4:6 bio-ink.
5) The inability of the 2:4:6 bio-ink to produce a complete monolayer suggested that the electrostatic repulsion must be addressed. Further research involving scaffolds treated with higher concentrations of poly(L-lysine) and for varying incubation times should be done to see if the electrostatic repulsion can be mitigated. If the poly(L-lysine) treatment is unable to mitigate the electrostatic repulsion, studies into the effect of removing ester sulfates from the surface of the CNCs should be done.
6) While not the original outcome desired in this research the ability of the bio-ink to repel cells has the potential to be used for micropatterning of cells. Further research should be done to investigate the bio-ink potential for cell patterning.

References

1. Canadian Cancer Society. *Canadian Cancer Statitistics 2017*. (2017). doi:10.1007/3-540-46877-3_22

2. DE ROSA, M. *et al.* Genetics, diagnosis and management of colorectal cancer (Review). *Oncol. Rep.* **34**, 1087–1096 (2015).

3. Brenner, H., Kloor, M. & Pox, C. P. Colorectal cancer. *Lancet* **383**, 1490–1502 (2014).

4. Statistics Canada. Annual Demographic Estimates : Canada , Provinces and Territories. (2019).

5. Jacques, F. *et al.* Colon and Rectum Cancer Staging. *Am. Cancer Soc.* 1 (2009).

6. Young, B., Kyung, H., Yong, W. & Beom, Y. Animal models of colorectal cancer with liver metastasis. *Cancer Lett.* **387**, 114–120 (2017).

7. van Marion, D., Domanska, U., Timmer-bosscha, H. & Walenkamp, A. Studying cancer metastasis : Existing models, challenges and future perspectives. *Crit. Rev. Oncol. / Hematol.* **97**, 107–117 (2016).

8. Golovko, D., Kedrin, D., Yilmaz, O. H. & Roper, J. Review: Colorectal cancer models for novel drug discovery. *Expert Opin Drug Discov* **10**, 1217–1229 (2015).

9. Young, M. & Reed, K. Organoids as a Model for Colorectal Cancer. *Curr. Colorectal Cancer Rep.* **12**, 281–287 (2016).

10. Edmondson, R., Broglie, J., Adcock, A. & Yang, L. Three-Dimensional Cell Culture Systems and Their Applications in Drug Discovery and Cell-Based Biosensors. *Assay Drug Dev. Technol.* **12**, 207–218 (2014).

11. Rmali, K., Puntis, M. & Jiang, W. Tumour-associated angiogenesis in human colorectal cancer. *Color. Dis.* **9**, 3–14 (2007).

12. Kim, Y. *et al.* Quantification of cancer cell extravasation in vivo. *Nat. Protoc.* **11**, 937–948 (2016).

13. Peddareddigari, V., Wang, D. & Dubois, R. The tumor microenvironment in colorectal carcinogenesis. *Cancer Microenviron.* **3**, 149–166 (2010).

14. Xiong, G. & Xu, R. Function of cancer cell-derived extracellular matrix in tumor progression. *J. Cancer Metastasis Treat.* **2**, 357 (2016).

15. Kirkland, S. Type I collagen inhibits differentiation and promotes a stem cell-like phenotype in human colorectal carcinoma cells. *Br. J. Cancer* **101**, 320–326 (2009).

16. Rabinovitz, I. & Mercurio, A. The integrin alpha6beta4 functions in carcinoma cell migration on laminin-1 by mediating the formation and stabilization of actin-containing motility structures. *J. Cell Biol.* **139**, 1873–84 (1997).

17. Zapatka, M. *et al.* Basement membrane component laminin-5 is a target of the tumor suppressor Smad4. *Oncogene* **26**, 1417–1427 (2007).

18. Ding, J., Li, D., Wang, X., Wang, C. & Wu, T. Fibronectin promotes invasiveness and focal adhesion kinase tyrosine phosphorylation of human colon cancer cell. *Hepatogastroenterology*. **55**, 2072–6

19. Yanagishita, M. Function of proteoglycans in the extracellular matrix. *Acta Pathol. Jpn.* **43**, 283–93 (1993).

20. Hashimoto, Y., Skacel, M. & Adams, J. Association of loss of epithelial syndecan-1 with stage and local metastasis of colorectal adenocarcinomas: An immunohistochemical study of clinically annotated tumors. *BMC Cancer* **8**, 1–7 (2008).

21. Kim, H. *et al.* Hyaluronan facilitates invasion of colon carcinoma cells in vitro via interaction with CD44. *Cancer Res.* **64**, 4569–4576 (2004).

22. Laurich, C. *et al.* Hyaluronan mediates adhesion of metastatic colon carcinoma cells. *J. Surg. Res.* **122**, 70–74 (2004).

23. Hemshekhar, M. *et al.* Emerging roles of hyaluronic acid bioscaffolds in tissue engineering and regenerative medicine. *Int. J. Biol. Macromol.* **86**, 917–928 (2016).

24. Murphy, S. & Atala, A. 3D bioprinting of tissues and organs. *Nat. Biotechnol.* **32**, 773–785 (2014).

25. Gu, B. *et al.* 3-Dimensional Bioprinting for Tissue Engineering Applications. *Biomater. Res.* **20**, 1–8 (2016).

26. Skardal, A. & Atala, A. Biomaterials for Integration with 3-D Bioprinting. *Ann. Biomed. Eng.* **43**, 730–746 (2015).

27. Zhang, K. *et al.* Acta Biomaterialia 3D bioprinting of urethra with PCL / PLCL blend and dual autologous cells in fibrin hydrogel : An in vitro evaluation of biomimetic mechanical property and cell growth environment. *Acta Biomater.* **50**, 154–164 (2017).

28. Vlaia, L., Coneac, G., Olariu, I., Vlaia, V. & Lupuleasa, D. Cellulose-Derivatives-Based Hydrogels as Vehicles for Dermal and Transdermal Drug Delivery. in *Emerging Concepts in Analysis and Applications of Hydrogels* **2**, 64 (InTech, 2016).

29. Koffler, J. *et al.* Biomimetic 3D-printed scaffolds for spinal cord injury repair. *Nat. Med.* **25**, (2019).

30. Shoulders, M. & Raines, R. Collagen Structure and Stability. *Annu. Rev. Biochem.* **78**, 929–958 (2009).

31. Wang, Y. *et al.* Biomaterials A microengineered collagen scaffold for generating a polarized crypt- villus architecture of human small intestinal epithelium. *Biomaterials* **128**, 44–55 (2017).

32. Gorgieva, S. & Kokol, V. Collagen- vs. Gelatine-Based Biomaterials and Their Biocompatibility: Review and Perspectives. in *Biomaterials Applications for Nanomedicine* 1–36 (InTech, 2011). doi:10.5772/24118

33. Yin, J., Yan, M., Wang, Y., Fu, J. & Suo, H. 3D Bioprinting of Low-Concentration Cell-Laden Gelatin Methacrylate (GelMA) Bioinks with a Two-Step Cross-linking Strategy.

ACS Appl. Mater. Interfaces **10**, 6849–6857 (2018).

34. Cyphert, J., Trempus, C. & Garantziotis, S. Size Matters: Molecular Weight Specificity of Hyaluronan Effects in Cell Biology. *Int. J. Cell Biol.* **2015**, 1–8 (2015).

35. Maleki, A., Kjøniksen, A. & Nyström, B. Anomalous viscosity behavior in aqueous solutions of hyaluronic acid. *Polym. Bull.* **59**, 217–226 (2007).

36. Cowman, M., Schmidt, T., Raghavan, P. & Stecco, A. Viscoelastic Properties of Hyaluronan in Physiological Conditions. *F1000Research* **4**, 1–13 (2018).

37. Highley, C., Rodell, C. & Burdick, J. Direct 3D Printing of Shear-Thinning Hydrogels into Self- Healing Hydrogels. doi:10.1002/adma.201501234

38. Andriamanantoanina, H. & Rinaudo, M. Relationship between the molecular structure of alginates and their gelation in acidic conditions. *Polym. Int.* **59**, 1531–1541 (2010).

39. Bouhadir, K. *et al.* Degradation of partially oxidized alginate and its potential application for tissue engineering. *Biotechnol. Prog.* **17**, 945–950 (2001).

40. Tabriz, A., Hermida, M., Leslie, N. & Wenmiao, S. Three-dimensional bioprinting of complex cell laden alginate hydrogel structures. *Biofabrication* **7**, 45012 (2015).

41. Zargar, V., Asghari, M. & Dashti, A. A Review on Chitin and Chitosan Polymers: Structure, Chemistry, Solubility, Derivatives, and Applications. *ChemBioEng Rev.* **2**, 204–226 (2015).

42. Demitras, T., Irmak, G. & Gumusderelioglu, M. A bioprintable form of chitosan hydrogel for bone tissue engineering. *Biofabrication* **9**, (2017).

43. Kamel, S., Ali, N., Jahangir, K., Shah, S. & El-Gendy, A. Pharmaceutical significance of cellulose: A review. *Express Polym. Lett.* **2**, 758–778 (2008).

44. Sannino, A., Demitri, C. & Madaghiele, M. Biodegradable cellulose-based hydrogels: Design and applications. *Materials (Basel).* **2**, 353–373 (2009).

45. Gershlak, J. *et al.* Biomaterials Crossing kingdoms : Using decellularized plants as perfusable tissue engineering scaffolds. *Biomaterials* **125**, 13–22 (2017).

46. Lin, N. & Dufresne, A. Surface chemistry, morphological analysis and properties of cellulose nanocrystals with gradiented sulfation degrees. *Nanoscale* **6**, 5384–5393 (2014).

47. Yang, J., Han, C. & Sun, R. Simple approach to reinforce hydrogels with cellulose nanocrystals. *Nanoscale* **6**, 5934–5943 (2014).

48. Ching, Y. *et al.* Rheological properties of cellulose nanocrystal-embedded polymer composites: a review. *Cellulose* **23**, 1011–1030 (2016).

49. Libanori, R. *et al.* Dynamics of Cellulose Nanocrystal Alignment. (2018). doi:10.1021/acsnano.8b02366

50. Wu, Y., Lin, Z., Wenger, A., Tam, K. & Tang, X. 3D bioprinting of liver-mimetic construct with alginate/cellulose nanocrystal hybrid bioink. *Bioprinting* **9**, 1–6 (2018).

51. Barnes, H., Hutton, J. & Walters, K. *An Introduction to Rheology*. (Elsevier, 1989).

52. Bruneaux, J., Therriault, D. & Heuzey, M. Micro-extrusion of organic inks for direct-write assembly. *J. Micromechanics Microengineering* **18**, 115020 (2008).

53. Oyen, M. Mechanical characterisation of hydrogel materials. *Int. Mater. Rev.* **59**, 44–59 (2014).

54. Reddy, N., Reddy, R. & Jiang, Q. Crosslinking biopolymers for biomedical applications. *Trends Biotechnol.* **33**, 362–369 (2015).

55. Shackelford, J. Chapter 6: Mechanical Behaviour. in *Introduction to Materials Science for Engineers* 152–209 (Pearson Education, Inc, 2009).

56. Shirahama, H., Lee, B., Tan, L. & Cho, N. Precise Tuning of Facile One-Pot Gelatin Methacryloyl (GelMA) Synthesis. *Nat. Publ. Gr.* 1–11 (2016). doi:10.1038/srep31036

57. Cheung, L. Properties of Hydrogels Incorporating Graphene Oxide-based Nanoparticles for Tissue Engineering Purposes by. (University of Waterloo, 2016).

58. Wu, Y. 3D Printing of Soft Hydrogels Incorporating Functional Nanomaterials. (University of Waterloo, 2016).

59. Blaeser, A. *et al.* Shear Stress in 3D-Bioprinting strongly impacts Human MSC Survival and Proliferation Potential. *BioNanoMat* **16**, 81–86 (2015).

60. Ouyang, L., Highley, C., Sun, W. & Burdick, J. A Generalizable Strategy for the 3D Bioprinting of Hydrogels from Nonviscous Photo-crosslinkable Inks. *Adv. Mater.* **29**, (2017).

61. Noshadi, I. *et al.* In vitro and in vivo analysis of visible light crosslinkable gelatin methacryloyl (GelMA) hydrogels. *Biomater. Sci.* **5**, 2093–2105 (2017).

62. Lim, K. *et al.* New Visible-Light Photoinitiating System for Improved Print Fidelity in Gelatin-Based Bioinks. *ACS Biomater. Sci. Eng.* **2**, 1752–1762 (2016).

63. Bishop, J., Schuksz, M. & Esko, J. Heparan sulphate proteoglycans fine-tune mammalian physiology. *Nature* **446**, 1030–1037 (2007).

Appendices

Appendix A: Polymer Mixing Order and its Effect on Viscosity

In the initial research into the use of GelMA in the alginate/CNC system the GelMA would be first dissolved in water before the addition of CNC which would form a very thin solution which would then thicken up with the addition of alginate. When this bio-ink was autoclaved for use with cells it was found to change colour from white to a light yellow suggesting a change in chemical composition. From autoclaving samples of the different polymers, it was found that the colour change came from GelMA (data not shown). When GelMA is heated it has a low viscosity making it possible to filter through a 0.22 µL filter. Alginate and CNCs on the other hand produce solutions that are too viscous to filter and therefor would still need to be autoclaved to make it sterile. Alginate and CNC were then mixed together and autoclaved before the addition of the filtered GelMA. It was at this point that a drastic change in viscosity was observed and an investigation into polymer mixing order was made. As can be seen in Figure 17 the dispersion of CNCs in water before the addition of alginate and then GelMA produced the highest viscosities across all shear rates. This is likely due to CNC's ability to be suspended in aqueous environments due the sulfate ester groups on the outside repelling the CNCs from each other before the introduction of

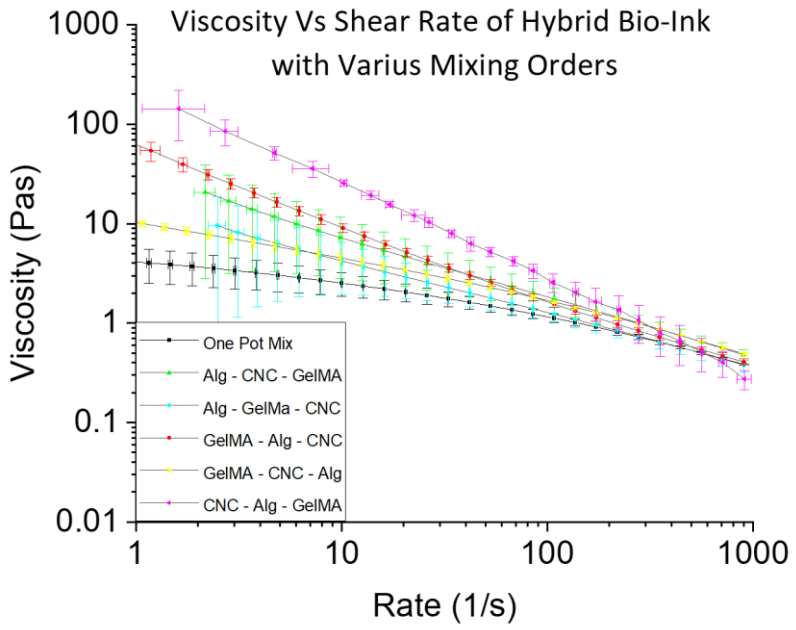

Figure 18: Viscosity vs shear rate of 2:4:6 bio-ink with different polymer mixing order.

amorphous have a chance to wrap around them. This would create a somewhat rigid polymer network increasing the viscosity of the bio-ink. This mixing order was adopted as it still produced shear thinning and would be more likely to maintain its shape throughout the printing process.

Appendix B: H-NMR Spectrums and DOS Calculations

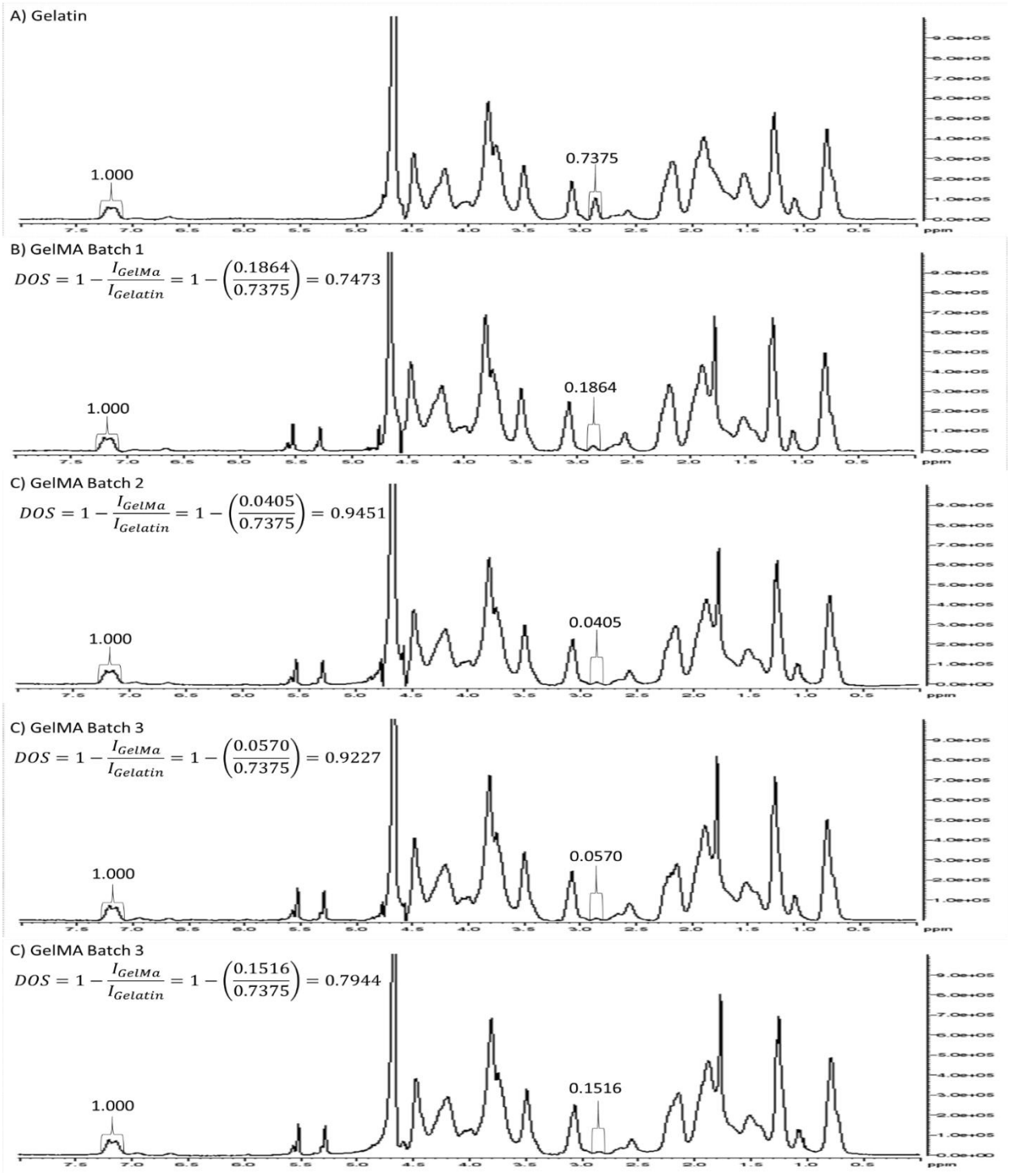

Figure 19: HNMR spectrums of different GelMA batches and DOS calculations.

Appendix C: Compression Data and Linear Model Fittings

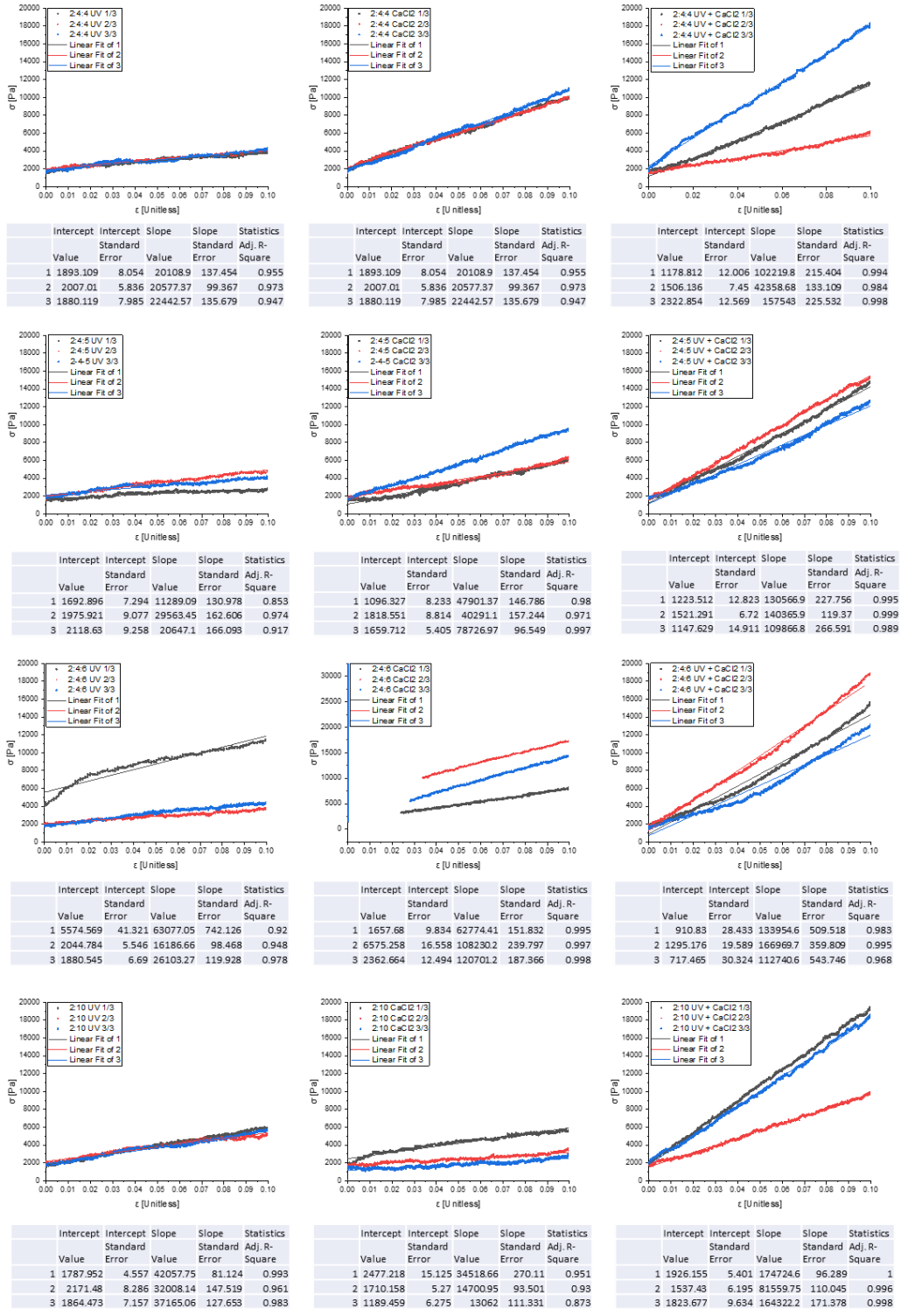

	Intercept Value	Intercept Standard Error	Slope Value	Slope Standard Error	Statistics Adj. R-Square
1	1893.109	8.054	20108.9	137.454	0.955
2	2007.01	5.836	20577.37	99.367	0.973
3	1880.119	7.985	22442.57	135.679	0.947

	Intercept Value	Intercept Standard Error	Slope Value	Slope Standard Error	Statistics Adj. R-Square
1	1893.109	8.054	20108.9	137.454	0.955
2	2007.01	5.836	20577.37	99.367	0.973
3	1880.119	7.985	22442.57	135.679	0.947

	Intercept Value	Intercept Standard Error	Slope Value	Slope Standard Error	Statistics Adj. R-Square
1	1178.812	12.006	102219.8	215.404	0.994
2	1506.136	7.45	42358.68	133.109	0.984
3	2322.854	12.569	157543	225.532	0.998

	Intercept Value	Intercept Standard Error	Slope Value	Slope Standard Error	Statistics Adj. R-Square
1	1692.896	7.294	11289.09	130.978	0.853
2	1975.921	9.077	29563.45	162.606	0.974
3	2118.63	9.258	20647.1	166.093	0.917

	Intercept Value	Intercept Standard Error	Slope Value	Slope Standard Error	Statistics Adj. R-Square
1	1096.327	8.233	47901.37	146.786	0.98
2	1818.551	8.814	40291.1	157.244	0.971
3	1659.712	5.405	78726.97	96.549	0.997

	Intercept Value	Intercept Standard Error	Slope Value	Slope Standard Error	Statistics Adj. R-Square
1	1223.512	12.823	130566.9	227.756	0.995
2	1521.291	6.72	140365.9	119.37	0.999
3	1147.629	14.911	109866.8	266.591	0.989

	Intercept Value	Intercept Standard Error	Slope Value	Slope Standard Error	Statistics Adj. R-Square
1	5574.569	41.321	63077.05	742.126	0.92
2	2044.784	5.546	16186.66	98.468	0.948
3	1880.545	6.69	26103.27	119.928	0.978

	Intercept Value	Intercept Standard Error	Slope Value	Slope Standard Error	Statistics Adj. R-Square
1	1657.68	9.834	62774.41	151.832	0.995
2	6575.258	16.558	108230.2	239.797	0.997
3	2362.664	12.494	120701.2	187.366	0.998

	Intercept Value	Intercept Standard Error	Slope Value	Slope Standard Error	Statistics Adj. R-Square
1	910.83	28.433	133954.6	509.518	0.983
2	1295.176	19.589	166969.7	359.809	0.995
3	717.465	30.324	112740.6	543.746	0.968

	Intercept Value	Intercept Standard Error	Slope Value	Slope Standard Error	Statistics Adj. R-Square
1	1787.952	4.557	42057.75	81.124	0.993
2	2171.48	8.286	32008.14	147.519	0.961
3	1864.473	7.157	37165.06	127.653	0.983

	Intercept Value	Intercept Standard Error	Slope Value	Slope Standard Error	Statistics Adj. R-Square
1	2477.218	15.125	34518.66	270.11	0.951
2	1710.158	5.27	14700.95	93.501	0.93
3	1189.459	6.275	13062	111.331	0.873

	Intercept Value	Intercept Standard Error	Slope Value	Slope Standard Error	Statistics Adj. R-Square
1	1926.155	5.401	174724.6	96.289	1
2	1537.43	6.195	81559.75	110.045	0.996
3	1823.677	9.634	164322.2	171.378	0.998

Figure 20: Compression data for bio-inks crosslinked with different mechanisms.